



An improved modelling chain for bias-adjusted high-resolution

climate and hydrological projections for Norway

- 3 Shaochun Huang¹, Wai Kwok Wong¹, Andreas Dobler³, Sigrid Jørgensen Bakke¹, Stein Beldring¹,
- 4 Ingjerd Haddeland^{1*}, Hans Olav Hygen³, Tyge Løvset², Stephanie Mayer², Kjetil Melvold¹, Irene Brox
- 5 Nilsen¹, Gusong Ruan¹, Silje Lund Sørland², Anita Verpe Dyrrdal³
- 6 Department of Hydrology, Norwegian Water Resources and Energy Directorate, Oslo, 0301, Norway
- 7 2NORCE Research AS, and Bjerknes Centre for Climate Research, Bergen, 5008, Norway
- 8 ³Department of Climate and Environment, Norwegian Meteorological Institute, Oslo, 0371, Norway
- 9 ^now at SWECO AS, Bergen, Norway
- *now at Lyse AS, Stavanger, 4018, Norway
- 11 Correspondence to: Shaochun Huang (shh@nve.no)

12 Abstract

13

14

15

1617

18

19

2021

22

23

24

25

26

27

2829

About every 10 years, the Norwegian Centre for Climate Services publishes a national climate assessment report, presenting the updated historical climate change and climate projections towards the end of this century. This paper documents the model experiment used to generate high-resolution climate and hydrological projections for the new climate assessment report published in October 2025. The model experiment follows the standard modelling chain for hydrological impact assessment, i.e., climate model selection - downscaling and bias adjustment - hydrological modelling. However, compared with the model experiment for the climate assessment report published in 2015, all modelling components have been improved in terms of data availability, data quality and methodology. Specifically, a large climate model ensemble was available and new criteria were developed to select tailored climate projections for Norway. Two bias-adjustment methods (one univariate and one multivariate) were applied to account for the uncertainty of method choice. The hydrological modelling was improved by implementing a physically-based Penman-Monteith method for evaporation and a glacier model accounting for glacier retreat under climate change scenarios. Besides model description, this paper elaborates the effects of different bias-adjustment methods and the contribution of climate models and bias-adjustment methods to the uncertainty of climate and hydrological projections under the RCP4.5 scenario as examples. The results show that the two bias-adjustment methods can contribute larger uncertainty to seasonal projections than climate models. The multivariate bias-adjustment method improves hydrological simulations, especially in the reference period, but cannot conserve climate change signals of the original climate projections. The dataset generated by the presented modelling chain provides the most updated, comprehensive and detailed hydrometeorological projections for mainland Norway, serving as a knowledge base for climate change adaptation to decision makers at various administrative levels in Norway.

and national climate risk adaptations (DCCEW, 2023).



32

33

42

43

44

45

46 47

48

49

50

51

52

5354



Key words: COR-BA-2025, distHBV-COR-BA-2025, RCP, CORDEX, EQM, 3DBC, distHBV, DEW, NORWAY

1 Introduction

34 It is unequivocal that human influence has warmed the climate at a rate that is unprecedented in at least the last 2000 years 35 (IPCC, 2021). The human-induced warming has already modified the global hydrological cycle, leading to significant shifts 36 in the spatial and temporal patterns of hydrological components (Gu and Adler, 2015; Gudmundsson et al., 2021; Li et al., 37 2023) and more intensive and frequent hydroclimatic extreme events (Alifu et al., 2022; Chinita et al. 2021; Dunn et al., 2020; 38 Padrón et al., 2020). These impacts pose unprecedented challenges for water resource management at regional and local scales, 39 and they are expected to be more severe in the future if unsustainable development continues (Wang and Liu, 2023). Therefore, 40 understanding of the potential climate change impact from a long-term and systematic perspective serves as a key basis to develop climate adaptation strategies, such as incorporating climate projections into European building standards (EEA, 2025) 41

General circulation models (GCMs) are important tools to understand and predict climate behavior under various greenhouse gas emission scenarios on the global scale. GCMs have been developed rapidly in the last decades, with an increasing number of models from over 40 within the Coupled Model Intercomparison Project phase 5 (CMIP5, Taylor et al., 2012) for Representative Concentration Pathway (RCP) emission scenarios to over 60 within CMIP6 (Eyring et al., 2016) for the Shared Socioeconomic Pathways (SSP) emission scenarios. Such a large ensemble of models provides valuable information of uncertainty for future climate projections, accounting for natural climate variability, unknown socio-economic developments, and model differences (Hawkins and Sutton, 2011). However, the use of the full ensemble can be challenging for impact models due to computational restrictions, so it often requires a careful selection of projections for specific study areas based on comprehensive analysis of the whole ensemble (Dalelane et al., 2018). In addition, GCM outputs are hardly applied for impact assessment at regional and local scales due to their coarse spatial resolutions (e.g., ~0.25 to 3° for the CMIP6 models and ~0.5 to 4° for the CMIP5 models) and systematic biases (Rössler et al., 2019), and they are usually downscaled to fine spatial resolutions and bias adjusted for climate impact assessment and adaptation planning (Martinich & Crimmins, 2019).

The GCM outputs can be downscaled dynamically using regional climate models (RCMs) or statistically based on statistical 55 56 relationships between coarse-resolution variables in GCMs and fine-resolution or local observations in the historical period 57 (Zhang et al., 2020). Various RCMs and statistical downscaling methods have been developed and applied to downscale the 58 GCM outputs, increasing the number of climate projections for region scales. For example, the European Coordinated Regional 59 Downscaling Experiment (EURO-CORDEX, Jacob et al., 2020) applies 11 RCMs to downscale the outputs from 14 GCMs to 60 0.11° (ca. 12.5 km) horizontal resolution. Due to the high computational cost and time consumption, each RCM is able to 61 downscale one or a few GCMs outputs, resulting in 30, 25 and 64 regional climate projections for Europe under the RCP2.6, 62 RCP4.5 and RCP8.5 scenarios, respectively. In contrast, statistical downscaling methods, which are often combined with bias





adjustment, can be easily applied for a large ensemble of GCMs due to low computational requirements and fast calculations,

and over 50 statistical downscaling methods have been applied for Europe (Gutiérrez et al., 2019).

Each downscaling method has its strengths and weaknesses. The dynamic downscaling ensures the physical relationships between climatic variables and spatial dependence, but it inherits significant biases from GCMs and requires further bias adjustment and/or statistical downscaling depending on the scale of impact studies (Hundecha et al., 2016; Maraun og Widmann, 2018). In contrast, the statistical downscaling usually outperforms the RCMs in terms of bias, but many methods downscale individual climatic variables independently (univariate) and can lead to inaccurate inter-variable dependence. Eum et al. (2020) demonstrated substantial impact of the univariate and multivariate statistical downscaling methods on reproduction of snowfall and recommended the use of the multivariate methods for climate change impact assessment in snow-dominated watersheds. Meyer et al. (2019) also found underestimation of snow accumulation (up to 50%) in alpine catchments when using univariate contra multivariate bias-adjustment approach, which can be attributed to less precipitation below temperatures of 0 °C.

Due to the large number of GCM projections and downscaling methods, as well as their strengths and weaknesses, to construct a downscaled and bias-corrected ensemble for specific regions is challenging. Different choices of GCM and downscaling methods can lead to considerably different local climate projections and thus contribute large uncertainty to local decision-relevant climate outcomes (Tang et al., 2016; Lafferty & Sriver, 2023). In addition, they result in different climate impact projections for streamflow (Key, 2022), flood hazard (Kundzewicz et al., 2017), agriculture (Li et al., 2023), ecosystem (Pourmokhtarian et al., 2016), etc, causing inconsistent impact assessments not only within each impact sector but also across sectors. Therefore, a consistent and tailored ensemble of regional climate projections is highly appreciated for each region and many countries have put great efforts to create national ensembles of climate projections (Golding et al., 2025), such as Switzerland (Fischer et al., 2022), Germany (Hübener et al., 2017), UK (Reyniers et al., 2025) and Australia (Peter et al., 2024).

Norway is located in the northern high latitudes, which have experienced the strongest warming since 1980 among all regions in the world, with warming trends spanning from 0.2 to more than 0.6 °C/decade (IPCC, 2021). The strong warming in the historical period raises great attention from both the scientific community and the public to future climate change and its impacts on hydropower production (about 90% of total power production in the country), winter tourism (skiing), and water related natural hazards (i.e., flood, drought, avalanche and landslide). However, it is specifically challenging to construct robust and reliable climate projections as well as hydrological impact projections in Norway, due to the high heterogeneity in topographic and hydroclimatological characteristics.

Norway is one of the most mountainous countries in Europe, with more than 90% of the landscape consisting of mountains.

The rugged topography leads to a complex spatial and temporal pattern of temperature and precipitation, varying with



94

95

96 97

98

99

100

101

102

103

104

105

106

107

108

109

110

111

112113

114

115

116

117

118

119

120

121

122

123



geographical position, elevation, aspect (slope direction), and slope angle (Dobrowski et al., 2009; Franke, 2024). The spatial resolutions of the state-of-the-art GCMs and RCMs are too coarse to provide sufficient spatial variations of climate for such complex terrain. In addition, these projections often show a cold bias for Norway (Wong et al., 2016), which for example leads to a prolonged snow season, low winter runoff and late snowmelt in hydrological projections (Nilsen et al., 2021).

In order to construct a consistent and tailored ensemble of national climate projections as well as hydrological projections for Norway, the Norwegian Centre for Climate Services (NCCS) brings together experts from the Norwegian Meteorological Institute, the Norwegian Water Resources and Energy Directorate (NVE), the Norwegian Research Centre (NORCE) and Bjerknes Centre for Climate Research, NCCS is responsible for the national climate assessment report, updated about every 10 years, which presents updated historical climate change and climate projections towards the end of this century and serves as a knowledge base for climate change adaptation to decision makers and planners at various administrative levels in Norway (Nilsen et al., 2022). The previous climate assessment report "Climate in Norway 2100" (Hanssen-Bauer et al., 2015; hereafter abbreviated CiN-2015), published in 2015, was based on 10 available GCM-RCM combinations within the CMIP5 and EURO-CORDEX frameworks. The projections were further re-gridded and bias-adjusted into 1 × 1 km resolution using empirical quantile mapping and forced the distributed version of the HBV (Hydrologiska Byråns Vattenbalansavdelningen, i.e. "The Hydrological Bureau's Water Balance Department") hydrological model (distHBV, Beldring et al., 2003) to generate hydrological projections. This spatial resolution is the result of the need to serve projections that can be used locally on the one hand, and availability of computational resources and reference datasets to produce daily maps for the whole of Norway on the other. During the last 10 years, all methods along the modelling chain, including GCMs, RCMs, climate model selections, statistical downscaling and bias correction, and hydrological models, have been further developed, and the observation data has been updated and improved. These developments promote the new generation of high-resolution and bias-adjusted climate and hydrological projections, which are more robust than the previous ones in CiN-2015.

In this paper, we present the full description of the methods to produce the updated downscaled and bias-adjusted climate projections and hydrological projections for the new climate assessment report for Norway "CiN-2025" (Dyrrdal et al., 2025), specifically focusing on selection of GCM-RCMs combinations, statistical downscaling and bias-adjustment and hydrological modelling. Section 2 introduces the study area and historical input data. The methods described include the overview of the whole modelling chain (Section 3), selection of atmospheric variables from a set of EURO-CORDEX simulations (Section 4), statistical downscaling and bias-adjustment method (Section 5) and hydrological modelling (Section 6). In Section 7 and 8, we present the climate and hydrological products and uncertainty analysis. Finally, we discuss the limitations of the methods and the potential applications of the products, and point out the way towards the next generation of national climate projections for Norway in Section 9.





2 Study area and historical data

2.1 Study area

The modelling domain of this study is the mainland of Norway and a few river catchments draining from neighbouring countries (Sweden and Finland) (Fig. 1), resulting in 354448 1x1 km² grid cells. Due to large variations in latitude and altitude, Norway exhibits six climate regimes according to the Köppen-Geiger climate classification (Beck et al., 2018), ranging from temperate climate along the west coast to polar climate in high mountains and in the north (Fig. 1). The average elevation of Norway is about 460 m, ranging from 0 along the coast to 2469 m at Galdhøpiggen in the center of the country. Open firm ground and forest are the two major land covers in Norway, accounting for 36% and 37.8% of the mainland area, respectively (Statistics Norway, 2025). There are also large areas of bedrock (8.5%), followed by water (6.2%), bogs (5.4%), agricultural land (3.5%) and built-up (1.7%). About 1% of mainland Norway is covered by glaciers (Fig. 1). The mean annual temperature in the current standard normal period 1991–2020 ranges from -9.5 to +9.5 °C (Tveito, 2021). The warmest areas are found in lower-lying areas in southern Norway, and particularly along the coast in the southwest, while the coldest areas are in the high mountains and inland areas of the north. Norway also exhibits large spatial variability in precipitation, ranging from 212 mm in southern parts of Northern Norway to 6130 mm close to the Ålfotbreen glacier in Western Norway. The wet areas along the west coast are exposed to migrating low pressure systems most often arriving from the west-southwest (Lutz et al., 2024).

We selected 85 and 38 catchments for calibration and validation of the hydrological model, respectively. All these catchments are near-natural catchments and 112 of the 123 catchments are smaller than 1000 km². The distribution of the catchments

represents various climate and hydrological regimes, geographic conditions and landscape types in Norway. The catchment

boundary is delineated by NVE and the gauges at the outlet of these catchments are shown in Fig. 1.



145



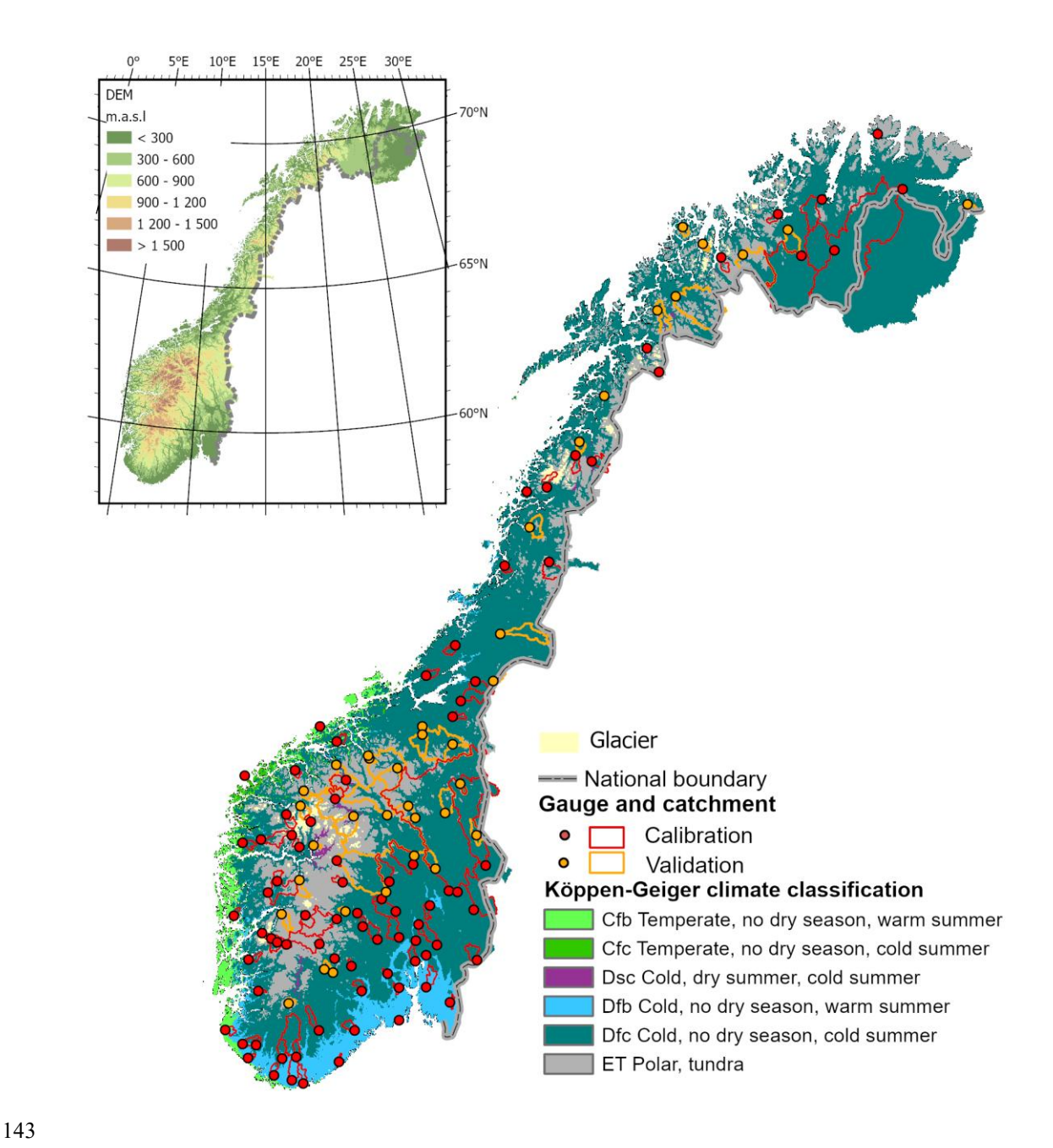


Figure 1: the climatic and topographic characteristics of the simulation domain as well as the locations of glaciers and hydrological gauging stations and catchment boundaries.





2.2 Historical meteorological data

- The historical meteorological data is used as reference in the bias-adjustment procedures and for hydrological model calibration and validations. It consists of nine atmospheric meteorological variables at a 1 x 1 km² grid covering Norway and river catchments in neighbouring countries (Fig. 1): mean, minimum and maximum 2m temperature (K), precipitation flux (mm/s), relative humidity (%), longwave and shortwave radiation (W/m²), pressure (Pa) and 10m wind speed (m/s).
- Daily minimum, maximum and mean temperatures as well as precipitation are provided by the seNorge2018 v20.05 dataset (Lussana et al., 2019; 2020). It covers the period 1957–2020 and is based on quality-assured daily datasets. The precipitation values are adjusted for wind-induced under-catch based on Wolff et al. (2015). Note that seNorge2018 continuously incorporates the latest available station data and is therefore not homogenized in time. This may affect the calculation of changes within the historical period.
- Daily wind speeds for Norway from 1958 to 2020 are obtained from the KliNoGrid 16.12 dataset. The KliNoGrid dataset is based on the Norwegian atmospheric reanalysis NORA10 (Reistad et al., 2011) wind speed data, downscaled onto a 1 km grid using a quantile mapping approach (Bremnes, 2004) to match the climatology of the high-resolution numerical weather prediction model AROME-MEtCoOp (Müller et al., 2017).
- Daily short- and longwave radiation, relative humidity and surface pressure are obtained from the HySN2018v2005ERA5 dataset. It is generated based on the ECMWF atmospheric reanalysis ERA5 (Herschbach et al., 2018) and seNorge2018 v20.05 and covers the period 1958–2020. The dataset is described in detail in Huang et al. (2022) and Erlandsen et al. (2021).

2.3 Data for setting-up hydrological models

To set up the hydrological model, a digital elevation model (DEM), as well as maps of soil type and land cover type with 1 km horizontal resolution are required. The DEM map was provided by the Norwegian Mapping Authority. Five soil types are reclassified based on the sediment map from the Geological Survey of Norway (Erlandsen et al., 2021), and bare mountain soil and moraine soils account for ca. 80% of the total mainland area. Nine land cover types (open area, bog, built-up, forest, cropland, heather, bedrock, lake, permanent ice and snow) are classified based on the National Land Resource Map (Ahlstrøm et al., 2014) and the remote sensing based forest resource map SAT-SKOG (Gjertsen and Nilsen, 2012). The forest land cover is further classified into 12 structural forest types to distinguish three species groups (spruce, pine, and deciduous forest) and four forest development stages (underdevelopment, two intermediate development stages and mature forest) (Majasalmi et al., 2018). The parametrization for each forest structural type, such as maximum leaf area index, vegetation height and shortwave albedo, is given by Majasalmi et al. (2018) and Bright et al. (2018). For glacier areas, the glacier modelling doesn't account for variation of soil types and uses simplified land cover types including open area, bog, forest, bedrock and glacier area coverage. However, it requires glacier ice thickness and glacier area data (Andreassen et al. 2015) to setup the model.





Discharge measurements from 123 gauging stations are used to calibrate and validate the hydrological model (Fig. 1). They are quality-assured by NVE. All 123 stations have measured daily discharge from 1980 to 2014 with less than 5% missing data. For the glacier modelling, mass balance data is only available for six glaciers and discharge measurements from 19 gauging stations downstream of the glaciers are used to calibrate and validate the hydrological model. All discharge and mass balance data are publicly available at sildre.nve.no and glacier.nve.no/glacier/viewer/ci/en/.

3 Modelling chain

We followed the commonly used modelling chain in hydrological climate impact studies, i.e., 1) emission scenarios, 2) GCMs and RCMs, 3) statistical downscaling and bias correction and 4) hydrological model (Fig. 2). The first component of the modelling chain is to select emission scenarios. For the CiN-2025 report, two RCPs used in CMIP5 were selected, representing a very stringent pathway (RCP2.6) and a moderate-emissions pathway (RCP4.5). The shared socioeconomic pathway SSP3-7.0 used in CMIP6 was selected to represent the high-emission scenario. The reason why only one SSP scenario was selected is that SSP1-2.6 and SSP3-7.0 were the first-priority scenarios for the EURO-CORDEX community (Katragkou et al., 2024). The data has become available late with regard to the time needed to run our complete modelling chain - it is in fact still not openly available - making the selection of more than one SSP scenario infeasible. Such a combination of CMIP5 and CMIP6 scenarios has also been used in other national climate projections, e.g., the climate projections in Switzerland published at the end of 2025 (Schumacher et al., 2024) which combined EURO-CORDEX RCP8.5 with CMIP6 SSP5-8.5 GCM simulations.





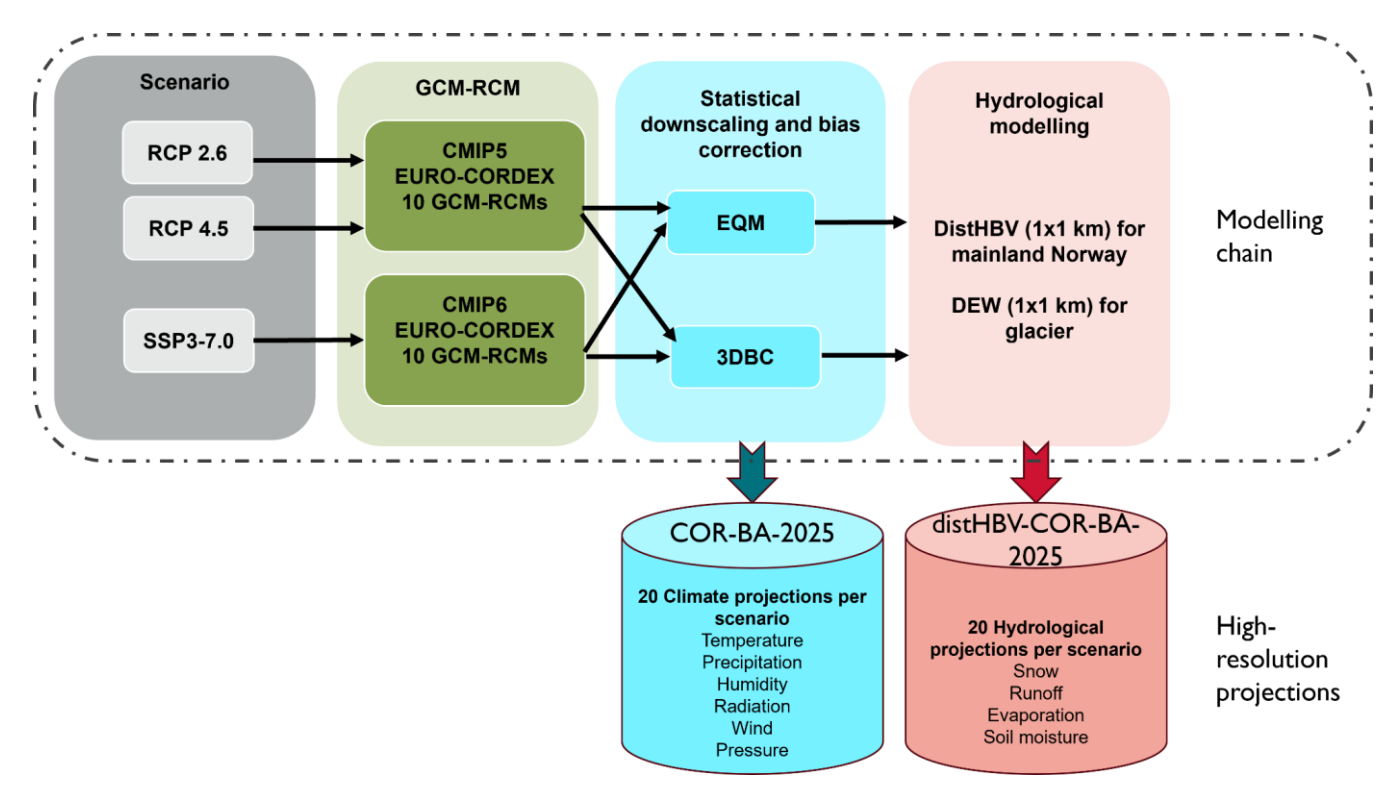


Figure 2: Modelling chain to generate high-resolution climate and hydrological projections for the CiN-2025 report.

In the second component of the modelling chain the task is to select a representative model ensemble from the EURO-CORDEX simulations (Jacob et al., 2014) for each emission scenario. Within the EURO-CORDEX framework, CMIP5 and CMIP6 GCMs are downscaled by different RCMs, resulting in a set of GCM-RCM combinations. For CiN-2025 a larger EURO-CORDEX ensemble for RCP scenarios was available compared to CiN-2015, enabling a more robust data basis and requiring new model selection strategies (Section 4).

Once the model ensemble was identified, the next step was to downscale the RCM projections of atmospheric variables from the original grid size of approximately 12.5 km to 1 km. It was followed by removal of biases in RCM simulations relative to observed meteorological data (Section 2.2) in the calibration period. For future projections, we adjusted the values based on the corrections established in the calibration period under the assumption that the relationship between the observed and modelled data remains unchanged. Two bias-adjustment methods were used: empirical quantile mapping (EQM) and three-dimensional bias-correction (3DBC) additionally to EQM (Section 5). The former is a widely used univariate bias-adjustment method and was used for CiN-2015. The latter adds a post-processing procedure, taking into account inter-variable dependencies. To our knowledge, this is the first time the 3DBC method is applied in Norway, and we have identified several strengths and weaknesses with this multivariate method (Section 5.3). Since the two bias-adjustment methods complement each other, we decided to apply both bias-adjustment methods on the RCM projections and provided two complete datasets





(EQM only and EQM with 3DBC). To assess the uncertainty in the climate and hydrological projections from the choice of methods, we have carried out an uncertainty analysis (Section 7.3 and 8.3).

The last component of the modelling chain is hydrological modelling. The distHBV model was still the main tool for simulating hydrological components under different climate scenarios for the CiN-2025 report, but two major improvements have been made since CiN-2015. The first improvement was to replace the temperature-based evaporation method with the Penman-Monteith equation in the distHBV model (Huang et al., 2019), because physical-based approaches, such as the Penman-Monteith method, consider more climatic variables and provide more robust changes in potential evaporation under climate scenarios than the empirical ones (McAfee, 2013; Tam et al., 2024). The second improvement was the inclusion of the Distributed Element Water balance model (DEW) (Beldring, 2008), which is an advanced version of distHBV in terms of the glacier module. Since distHBV was not able to simulate the changes in glacier area, glacier melt water can be unrealistically high under climate scenarios used in CiN-2015. In contrast, DEW is able to simulate glacier area, volume and surface elevation dynamically and thus gives more reliable hydrological projections under climate change for glacierized regions. Both models ran at 1 km spatial resolution and with daily time steps, but distHBV ran for all grid cells in Norway and DEW only ran for the grid cells covering glacierized regions. The smallest glaciers (< 1 km²) were omitted in the DEW model.

The modelling chain resulted in two datasets with a spatial resolution of 1x1 km at daily time steps, which will be serving as the basis for climate impact assessment in mainland Norway. The first dataset is termed COR-BA-2025 (short for CORDEX-Bias Adjusted, updated in 2025), consisting of 20 bias-adjusted high-resolution climate projections for each emission scenario and is available from 1970 to 2100 (2098 depending on GCMs). These projections include nine atmospheric variables at 1x1 km spatial resolution and with daily time steps: mean, minimum and maximum 2m temperature (K), precipitation flux (mm/s), relative humidity (%), longwave and shortwave radiation (W/m²), surface air pressure (Pa) and 10m wind speed (m/s). The second dataset is called distHBV-COR-BA-2025 and consists of 20 hydrological projections for each emission scenario at the same spatial and temporal resolution and coverage as the atmospheric projections. The hydrological projections include two flux variables (runoff and evaporation) representing average values over each grid cell in mm/day, and two state variables (soil moisture and snow water equivalent), which describe the average condition of the hydrological components in a grid cell with unit mm. The evaporation, soil moisture and snow water equivalent projections were generated by distHBV, whereas the runoff projections were obtained by superimposing the results of the glacierized grid cells from the DEW model on the runoff projections from distHBV.

To select the climate ensembles and assess future changes in climate and hydrology, we defined one reference period (1991–2020) and two future periods (2041–2070 and 2071–2100). The reference period was selected by two factors: 1) a recent climate period better represents today's climate, and 2) 1991–2020 is the current standard normal period defined by the World Meteorological Organization (WMO). However, in CMIP5 and CMIP6, the historical simulation runs end in 2005 and 2014,





respectively. Data from the emission scenario RCP4.5 was used to extend the historical period beyond 2005 for RCPs and the data from the emission scenario SSP3-7.0 was used to extend the historical period beyond 2014 for SSPs.

Since the main focus of this paper is on the description of the methods in the modelling chain rather than assessing climate and hydrological projections under different emission scenarios, we only present the methods and results for the RCP4.5 scenario as examples in the following sections. However, the methods described in this paper are valid for all three scenarios.

4 Selection of GCM-RCM combinations

Currently, the EURO-CORDEX CMIP5 projections comprise the largest high-resolution regional climate model ensemble for Europe and Norway. There are 17 identical model combinations based on the representative concentration pathways RCP2.6, RCP4.5 and RCP8.5. Based on all 17 models for RCP4.5, the projected temperature and precipitation changes in Norway ranges from 0.5 to 3.4 °C and from -2.6 to 12.5 % (indicated as grey shaded area in Fig. 3), respectively.

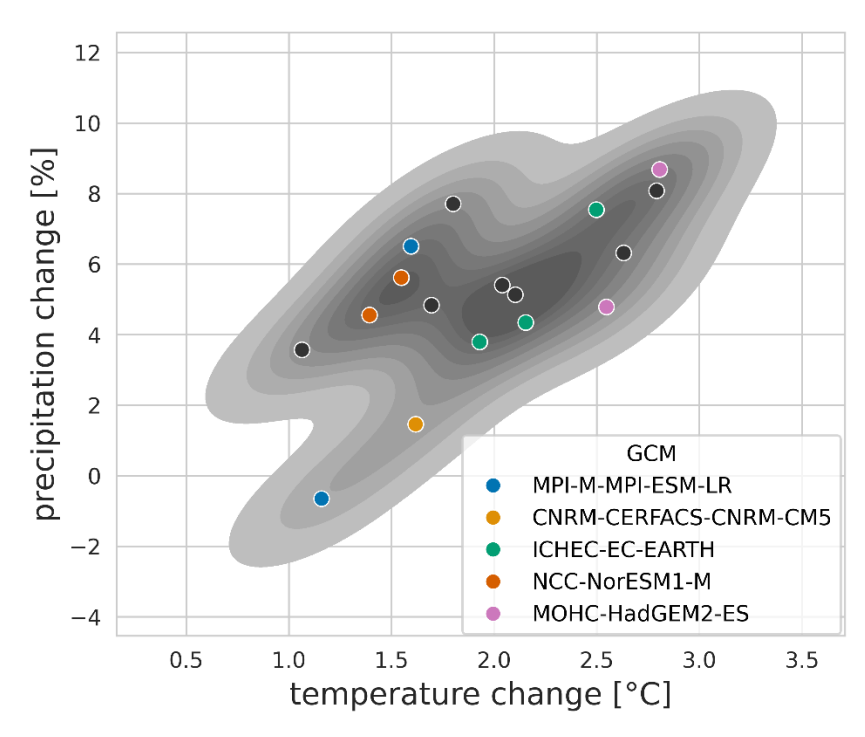


Figure 3. Projected changes in temperature and precipitation for mainland Norway by the end of the century (2071–2100 minus 1991–2020) under the RCP4.5 scenario (all dots). The grey shaded area indicates the distribution (kernel density estimate) of the projected changes comprising all 17 GCM-RCM combinations that were considered. The individual coloured points highlight the ten simulations selected for CiN-2025 (Table 1).





- Given time and computational constraints, we defined an upper limit of ten model combinations that are used as forcing data for the hydrological models. The ten GCMs-RCMs combinations were chosen based on the five following criteria:
 - 1) High-resolution (0.11 x 0.11°) simulations based on the representative concentration pathways RCP2.6, RCP4.5 and RCP8.5 are available on the Earth System Grid Federation (ESGF).
 - 2) Important physical phenomena in the GCMs such as temperature and precipitation cycles, circulation and storm tracks over Europe are represented in an acceptable manner, i.e. the chosen GCM scores satisfactory for at least two of the physical phenomena (Table 6 in McSweeney et al., 2015).
 - 3) Include as many plausible GCMs as possible that fulfil criteria 2 in order to capture the potential impact of the projected climate change signal.
 - 4) The GCM-RCM combination should be ranked in the 'best half' for 24 variables and impact-based indices (Table 2 in Vautard et al., 2020) for the region of Scandinavia (Figure 12a in Vautard et al., 2020).
 - 5) The temperature and precipitation biases for Norway, i.e. simulated vs. observed values from seNorge2018 v20.05 from 1971–2000 should not be visually striking compared to the biases in all available model combinations.

The selected model-combinations based on these five criteria are presented in Table 1. The projected changes in temperature and precipitation are shown for each model combination in Fig. 3. In total, these model combinations consist of five GCMs and six RCMs. Based on the selection of the ten GCM-RCM combinations (coloured dots in Fig. 3), the projected changes in temperature and precipitation in Norway range from 1.15 °C to 2.8 °C and from -1 % to 9 % in the future period 2071–2100 relative to the reference period 1991–2020.

The selected GCM-RCM combinations vary in data coverage and quality (Table 1). The GCM MOHC-HadGEM2-ES lacks 13 months towards the end of the time series, so we only used the simulations forced by this GCM until the end of 2098. When looking at near (2041–2070) and far future (2071–2100) changes, the MOHC-HadGEM2-ES simulations were shifted by two years, i.e. the periods for MOHC-HadGEM2-ES were 2039–2068 and 2069–2098. In addition, MOHC-HadGEM2-ES simulates 360 days instead of 365 (366) days. To fill in the missing five days, we simply copied the day number 150, 210, 240, 300 and 360 from the 360-day year and added these extra days to the day number 151, 212, 243, 304 and 365 in a normal year. For a leap year, a copy of day number 59 was added similarly. This simple technique was also used on NCC-NorESM1-M coupled with SMHI-RCA4 as this model combination does not support leap years. Unrealistically large snow accumulation at isolated grid cells have been discovered in the simulations from SMHI-RCA4 and DMI-HIRHAM5. They were considered as minor quality issues and their effects were reduced by applying a spatial smoothing on the variables minimum, mean and maximum temperature, and humidity, an approach adopted from CH2018 (2018).





Table 1. Summary of GCM-RCM combinations for RCPs which were selected for downscaling and bias-adjustment for the mainland of Norway. ¹: Original data has 360 days only. Additional days added. ²: Leap-year days added. ³: Spatial smoothing applied to tasmin, tasmax, tas and hurs

| Model combination name | GCM model id (CMIP5) | RCM model id (CORDEX) | Data coverage |
|----------------------------------|-----------------------|-----------------------|---------------|
| cnrm-rlilp1-aladin | CNRM-CERFACS-CNRM-CM5 | CNRM-ALADIN63 | 1960–2100 |
| ecearth-r12i1p1-rca ³ | ICHEC-EC-EARTH | SMHI-RCA4 | 1970–2100 |
| ecearth-r12i1p1-cclm | ICHEC-EC-EARTH | CLMcom-CCLM4-8-17 | 1960–2100 |
| ecearth-r3i1p1-hirham | ICHEC-EC-EARTH | DMI-HIRHAM5 | 1960–2100 |
| hadgem-rlilpl-rca ^{1,3} | MOHC-HadGEM2-ES | SMHI-RCA4 | 1970–2098 |
| hadgem-rlilpl-remo ¹ | MOHC-HadGEM2-ES | GERICS-REMO2015 | 1960–2098 |
| mpi-rlilp1-cclm | MPI-M-MPI-ESM-LR | CLMcom-BTU-CCLM4-8-17 | 1960–2100 |
| mpi-r2i1p1-remo | MPI-M-MPI-ESM-LR | MPI-CSC-REMO2009 | 1960–2100 |
| noresm-rlilp1-rca ^{2,3} | NCC-NorESM1-M | SMHI-RCA4 | 1970–2100 |
| noresm-r1i1p1-remo | NCC-NorESM1-M | GERICS-REMO2015 | 1960–2100 |

5 Downscaling and bias-adjustment methods

For CiN-2015, only daily mean temperature and precipitation were bias-adjusted, but for CiN-2025, nine surface variables from the RCM outputs were downscaled and bias-adjusted, namely mean, minimum and maximum air temperature at two meters height, precipitation, mean wind speed at 10 meters height, long- and shortwave radiation, surface pressure, and relative humidity at two meters height.

The nine climate variables from the RCM outputs were firstly re-gridded to the seNorge grid with a 1 km spatial resolution using nearest-neighbour method. This conservative way to downscale from a coarse to fine scale grid ensures that the original model outputs are preserved and not altered unintentionally by the downscaling step. The bias-adjustment procedure was then implemented on the grid cell basis. Depending on the variable adjusted, different reference datasets (see Section 2.2) were





used for calibration. Wet-day correction has also been applied prior to bias-adjustment of precipitation because RCMs generally provide more rainy days than the observed ones (Frei et al., 2003).

Since the grid cells are bias-adjusted individually, we need to select methods that are computational efficient, or at least applicable, and numerically stable (François et al., 2020) for a large number of grid cells (354 448 in total). We have tested a few bias-adjustment techniques categorized as quantile mapping (Cannon et al., 2015) and multivariate approaches (François et al., 2020). In the end, the univariate bias-adjustment adopting empirical quantile mapping (EQM) approach (Gudmundsson et al., 2012) was used to bias-adjust one climate variable at a time because the method meets all the aforementioned criteria and is widely used in adjusting climate model data. The results were further post-processed with the multivariate 3DBC approach (Mehrota and Sharma, 2019) to rectify inter-variable and spatial dependency structures.

5.1 EQM

The quantile mapping approaches establish a statistical transfer function for a variable between RCM outputs and observations in the calibration period 1985–2014, which is assumed to be valid for use in the projection period. Specifically, for EQM, 12 calendar-month-specific transfer functions were derived by fitting the empirical cumulative distribution functions (eCDFs) of the modelled values with the eCDFs based on observations for each grid cell. Daily data within a 3-month window centred on the month of interest were pooled and used to develop monthly eCDF to avoid overfitting (Cannon et al., 2015). For example, data from February to April were used to develop the eCDF for March. The transfer function was approximated by a series of empirical quantiles with fixed intervals of 0.01 spanning the probability space (0,1) (Gudmundsson et al., 2012). Only the 1st to 99th quantiles were obtained and used. Linear interpolation was applied for values in between those fixed quantiles. For values smaller than the 1st quantile and larger than the 99th quantile, constant linear extrapolation based on the 1st and 99th quantiles was performed accordingly.

The projection period starting from 2015 to 2100 was further divided into seven overlapping 30-year time slices. The first time slice, however, only covers 2015-2040, followed by 2021-2050, 2031-2060, etc. After the bias-adjustment of each time slice using the established transfer functions on a monthly basis, only the 10-year results in the middle of the period were being kept. For the first and the last time slices, the results of the first 16 years and the last 20 years were used respectively. A continuous time series covering the whole projection period was put together afterwards.

To reduce the potential impact of over-adjustment (modifying the long-term linear trend) and extrapolation (model-projected values lying outside the range of the historical distribution), the long-term mean of the projected period was first removed from model-projected values. This shifting of the future distribution can better secure the applicability of the transfer function based on historical distribution. The long-term mean was later reimposed after the bias-adjustment of the 'residuals'. For all the variables other than temperatures, long-term mean removal and reimposition were performed multiplicatively (see Cannon et





- al., 2015, for more details). Similar linear trend removal and reimposition for the projected values of temperature variables
- 328 were done additively.

329 **5.2 3DBC**

346

347

330 The bias-adjusted climate projections obtained from the univariate EQM approach were further processed with an additional 331 step to impose inter-variable, temporal and spatial dependency structures. The multivariate method we used is called 3DBC 332 (three-dimensional bias-correction) as it adjusts along the three dimensions: variables, time and space. It is described in detail 333 in Mehrotra and Sharma (2019). 3DBC is re-establishing the spatial, temporal and inter-variable structures from the reference 334 data by reordering the daily EQM values according to observed time-ranks at each grid-point, resulting in the bias-adjusted 335 data having the same rank structure (ordering) as the reference data in the calibration period. Compared to other multivariate 336 bias correction methods (e.g. the MBCn method developed by Cannon, 2018) the computational requirements of 3DBC are 337 relatively small, making its application on a large number of grid cells feasible. Note that 3DBC adjusts the ranks for future 338 periods according to changes in the variable auto-correlations as simulated by the RCMs. Thus, it does not strictly assume that 339 the dependency structures remain stable in future climates. However, while the original implementation by Mehrotra and 340 Sharma (2019) works on single calendar days across a future period of 30 years, our future period (2021-2100) consists of 80 341 years. Following the original approach would have resulted in imposing observed trends repeatedly on the future period. We 342 thus adapted the 3DBC method to work within single years of the EQM data, an ansatz that maintains the climate change 343 signals from the RCMs (and EQM) on an annual scale. As a result, the adjustments in the variable auto-correlations for the 344 future periods have a limited effect and do not fully transfer the dependency structure changes from the RCMs to the 3DBC 345 bias-adjusted data.

5.3 Evaluation of bias-adjustment methods

5.3.1 Performance of bias-adjustment methods

- Thorarinsdottir et al. (2013) proposed the use of integrated quadratic distance (IQD) as a performance measure to compare the
- full distribution of climate model output to the corresponding distribution of observed data. IQD was further employed by
- Yuan et al. (2019; 2021) to assess the performance of different bias-adjustment approaches. IQD (Eq. 1) is defined as:

351
$$d_{IQ}(F,G) = \int_{-\infty}^{+\infty} (F(t) - G(t))^2 dt$$
 (1)

- where F, G are two cumulative distribution functions. $d_{IO}(F, G)$ summarizes the differences, and a lower value implies a
- smaller difference between F and G. $d_{IO}(F, G) = 0$ if F = G. For further details, please see Thorarinsdottir et al. (2013). In this
- study, we compared the eCDFs of bias-adjusted precipitation and temperature with corresponding seNorge2018 v20.05 data
- over the calibration (1985–2014) and validation (1960–1984 or 1970–1984 depending on the period start of the RCM) periods





in each grid cell. In addition, we calculated IQD scores derived from comparison of original RCM outputs with the observed data.

IQD scores presented in Table 2 are averaged over all grid cells and GCM-RCM combinations. We evaluated and ranked the bias-adjustment methods according to the IQD scores averaged on an annual and seasonal basis. The results clearly demonstrate that both bias-adjustment approaches are far better at reproducing the full distributions of observed precipitation and temperature by several orders of magnitude than the original RCM outputs. As expected, the improvements are larger (smaller d_{IQ}) in the calibration period than the validation period. Furthermore, 3DBC performs better overall than EQM on seasonal results because 3DBC utilizes additional information about the intra-annual order of the observed time series in the post-processing, whereas the annual results remain the same. Thus, 3DBC provides added value as compared to EQM when seasonal statistical properties are of importance.

Table 2: Integrated quadratic distance (IQD) scores comparing eCDFs derived from two bias-adjustment approaches (EQM and 3DBC) in addition to original RCM outputs with reference datasets seNorge2018 v20.05 over the calibration (1985–2014) and validation (1960/70–1984) periods. All IQD scores are averages over all grid cells and GCM-RCM combinations. The best performance on each time scale is indicated in bold italic.

| | Calibration | | | Validation | | |
|---------------|-------------|----------|----------|------------|----------|----------|
| | Original | EQM | 3DBC | Original | EQM | 3DBC |
| Precipitation | | | | | | |
| Annual | 1.17E-01 | 2.27E-05 | 2.27E-05 | 1.32E-01 | 7.19E-03 | 7.19E-03 |
| Winter (DJF) | 1.61E-01 | 1.65E-03 | 5.61E-04 | 1.87E-01 | 2.90E-02 | 8.42E-03 |
| Spring (MAM) | 1.16E-01 | 6.42E-04 | 2.50E-04 | 1.52E-01 | 2.04E-02 | 5.22E-03 |
| Summer (JJA) | 1.34E-01 | 1.21E-03 | 3.50E-04 | 1.47E-01 | 1.11E-02 | 8.09E-03 |





| Autumn (SON) | 1.60E-01 | 1.03E-03 | 3.79E-04 | 1.42E-01 | 1.37E-02 | 1.04E-02 | |
|--------------|----------|----------|----------|----------|----------|----------|--|
| Temperature | | | | | | | |
| Annual | 1.81E-01 | 9.98E-05 | 9.98E-05 | 1.91E-01 | 1.37E-02 | 1.37E-02 | |
| Winter (DJF) | 3.59E-01 | 1.71E-03 | 1.40E-03 | 4.26E-01 | 7.73E-02 | 5.21E-02 | |
| Spring (MAM) | 3.00E-01 | 3.40E-03 | 1.06E-03 | 2.97E-01 | 2.77E-02 | 1.84E-02 | |
| Summer (JJA) | 5.72E-01 | 1.59E-03 | 7.09E-04 | 6.38E-01 | 3.03E-02 | 2.41E-02 | |
| Autumn (SON) | 1.79E-01 | 1.69E-03 | 9.86E-04 | 1.82E-01 | 1.81E-02 | 1.45E-02 | |

3DBC as a post-processing procedure follows the ranks of observed precipitation and temperature. It reorders the modelled results accordingly and can simulate the spatial correlation structures between these two variables in the historical period better than EQM can achieve. EQM inherits the spatial rank correlation pattern from the RCM. The seasonal differences between these two methods are often most pronounced in winter (DJF) and summer (JJA). Figure 4 shows an example for winter, comparing the bias-adjusted datasets from EQM and 3DBC with the reference datasets for calibration (1985–2014) and validation (1960–1984) periods for one RCM. EQM generally overestimates the rank correlations between precipitation and temperature almost over the whole country in winter. And this spatial rank correlation pattern seems to be rather stable from one period to another. Generally, the results confirm that 3DBC performs better in recovering the inter-variable spatial dependency structure.



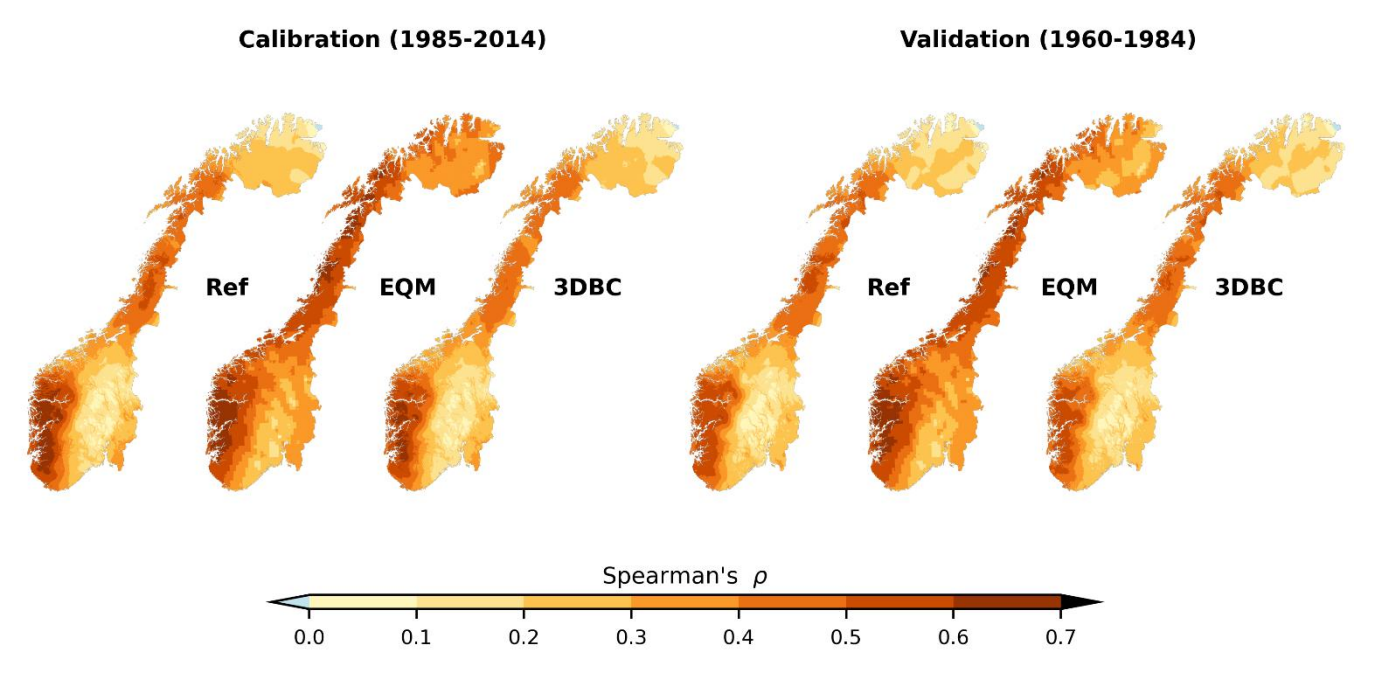


Figure 4: Rank correlation of daily precipitation and temperature in winter (DJF) for the two bias-adjustment methods. For calibration (1985–2014) and validation (1960–1984) periods, the two bias-adjusted datasets, EQM and 3DBC are based on historical run from mpi-r1i1p1-cclm and compared with reference datasets seNorge2018 v20.05.

5.3.2 Climate change signal preservation

When comparing the two methods of bias-adjustment in terms of climate change signals, EQM preserves the original climate change signals from the climate models better than 3DBC (Fig. 5). For precipitation, the larger increase in relative changes in winter for 3DBC than EQM are offset by smaller increases in relative changes in spring and summer. Changes in temperature show similar characteristics. Larger positive winter temperature changes for 3DBC are compensated by smaller positive spring temperature changes. The spreads of the changes are comparable between EQM and the original model outputs. 3DBC, on the other hand, exhibits varying spreads depending on the seasons and variables, as the climate change signal preservation is not strictly prescribed in the method. On an annual basis, these two methods provide identical results since 3DBC uses the same bias-adjusted results from EQM before further post-processing. By reshuffling the chronological order intra-annually, 3DBC modifies the seasonal change signals substantially.





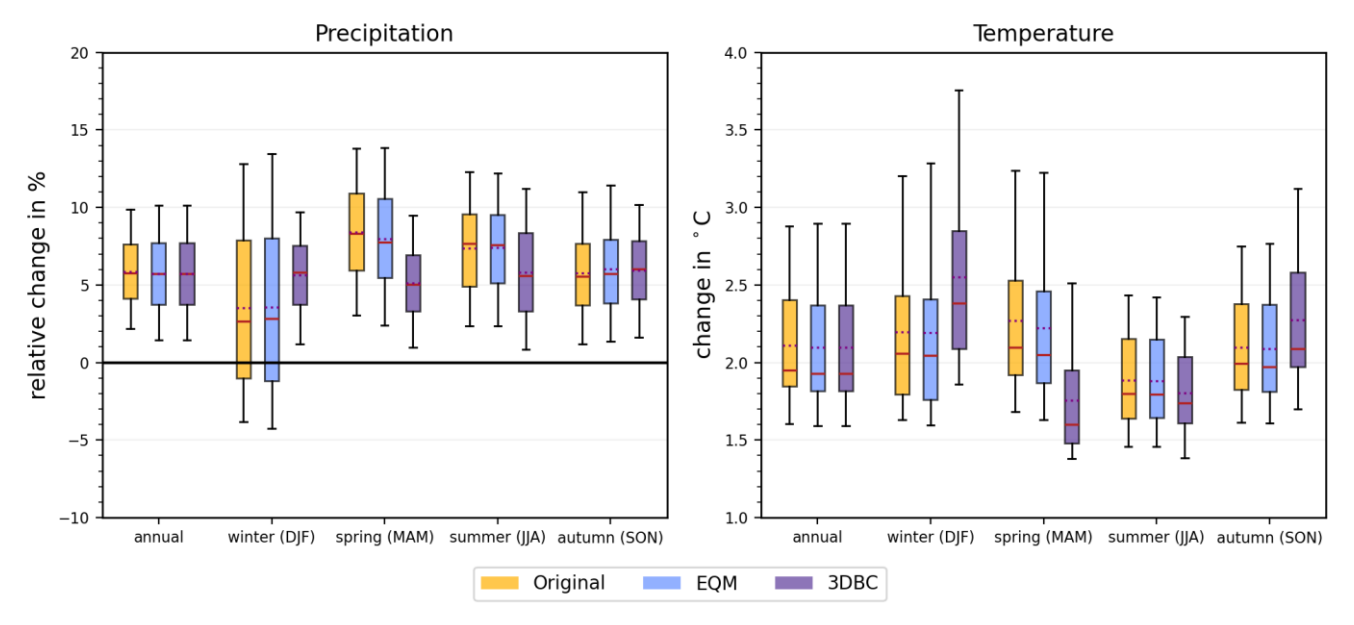


Figure 5: Comparison of projected annual and seasonal changes in precipitation (relative change in %, left panel) and temperature (change in °C, right panel) from 1991–2020 to 2071–2100 for RCP4.5. Results averaged over all grid cells and RCM model ensemble from two bias-adjustment procedures, EQM and 3DBC, are compared to the original RCM projections. The thick red line on the box indicates the median value whilst the dotted line represents the mean. The lower and upper boundaries of the box are the 25th and 75th percentiles. The lower and upper ends of the whiskers refer to the 5th and 95th percentiles.

6 Hydrological modelling

6.1 DistHBV

DistHBV is a spatially distributed version of the HBV precipitation-runoff model (Beldring et al., 2003) and is the major tool applied to assess hydrological responses to climate change in Norway. The model calculates the water balance for 1 x 1 km grid cells at a daily time step covering the entire mainland surface area of Norway and upstream areas in Finland and Sweden contributing to streamflow in Norwegian catchments. Each grid cell includes one soil type and up to five land cover types. DistHBV has components for accumulation, sub-grid scale distribution and ablation of snow, interception storage, sub-grid scale distribution of soil moisture storage, evapotranspiration, groundwater storage and runoff response, lake evaporation and glacier mass balance. The newly implemented Penman-Monteith method and the prescribed parameterizations are presented in Huang et al. (2019) and Erlandsen et al. (2021).

As for other conceptual hydrological models, calibration is necessary to adjust the DistHBV parameters to improve the model performance of reproducing observed discharge, due to the absence of directly measured catchment characteristics, natural variability and the non-linearity of the processes involved. Since all parameters to calculate potential evaporation are prescribed



414

415

416

417 418

419

420

421

422

423

427

428

429

430

431

432

433

434



412 in the Penman-Monteith equation, the calibration parameters are mainly associated with lake, subsurface and snow processes.

There are ten main calibration parameters (Table 3), of which three are land use specific and six are soil-specific, resulting in

a total of 44 parameters.

Table 3: list of calibration parameters. Note that the parameters in the landuse and soil categories vary across land use and soil types, respectively.

| Category | Parameter | Explanation | Unit | Min | Max |
|----------|-----------|---|------|----------|------|
| Lake | KLAKE | Rating curve constant | - | 1.00E-04 | 0.1 |
| | SMELT_T | Snow melt temperature | °C | -1 | 2 |
| | SMELTR | Temperature index for snow melt rate | m/°C | 1.00E-04 | 0.01 |
| Landuse | IMELTR | Ice melt rate for glaciers additional coefficient to SMELTR | - | 1 | 4 |
| | FC | Field capacity | m | 1.00E-02 | 1 |
| | BETA | Shape coefficient of soil moisture | - | 1 | 5 |
| | KUZ | Upper zone recession coefficient | - | 1.00E-03 | 1 |
| | ALFA | Upper zone nonlinear drainage coefficient | - | 1 | 2 |
| | PERC | Percolation from upper zone to lower zone | - | 1.00E-03 | 0.5 |
| Soil | KLZ | Lower recession coefficient | - | 1.00E-03 | 1 |

The model was calibrated against discharges at 85 gauges (Fig. 1) from 2000 to 2007 using the parameter estimation routine PEST (Doherty and Skahill, 2006) and a multi-criteria calibration approach (Huang et al., 2019). The multi-criteria include the Nash and Sutcliffe efficiency (NSE) (Nash and Sutcliffe, 1970), the bias in water balance (BIAS) and the volume bias in the high-flow segment of the flow duration curve (ΔFHV , 0 – 0.02 flow exceedance probabilities) (Yilmaz et al., 2008). Since PEST minimizes the difference between the criteria results and their ideal values (1 for NSE and 0 for biases), the calibration objective function θ containing the three criteria at multiple gauges can be formulated as Eq. 2.

424
$$\theta = W_{NSE} * \sum_{i=1}^{n} (1 - NSE_i)^2 + W_{BIAS} * \sum_{i=1}^{n} (BIAS_i)^2 + W_{\Delta FHV} * \sum_{i=1}^{n} (\Delta FHV_i)^2$$
 (2)

425 where W are weights for each criterion and n = 85, the number of calibration catchments. W_{NSE} equals to 8 and W_{BIAS} and 426

 $W_{\Lambda FHV}$ equal to 1 to achieve a good calibration performance.

Five PEST runs were carried out with different initial parameter values and only the parameter set giving the best model performance was selected for model validation. The model was validated against the discharge of the 85 calibration stations and additional 38 gauging stations from 2008 to 2014 to evaluate the temporal and spatial transferability of the model, respectively. Finally, long-term model performance is assessed based on the discharge of all 123 gauges from 1981 to 2014. Figure 6 shows the calibration and validation results in terms of NSE and BIAS. During the calibration period, about 50% and 29% of the catchments show good (NSE>0.65 and |BIAS|<0.1) and satisfactory (0.65>NSE>0.55 and 0.1<|BIAS|<0.15) results (Moriasi et al., 2007), respectively. The model generally underestimates discharge with the median bias of -5%, mainly due to underestimation of precipitation in seNorge2018 v20.05 data. The model performs similarly in terms of median NSE in the





validation period for the 85 gauging stations, but underestimates the discharge for about 75% of the 38 gauges. Nevertheless, the validation results for the whole historical period (1981–2014) are similar to the calibration results in terms of both NSE and BIAS, indicating a robust long-term model performance.

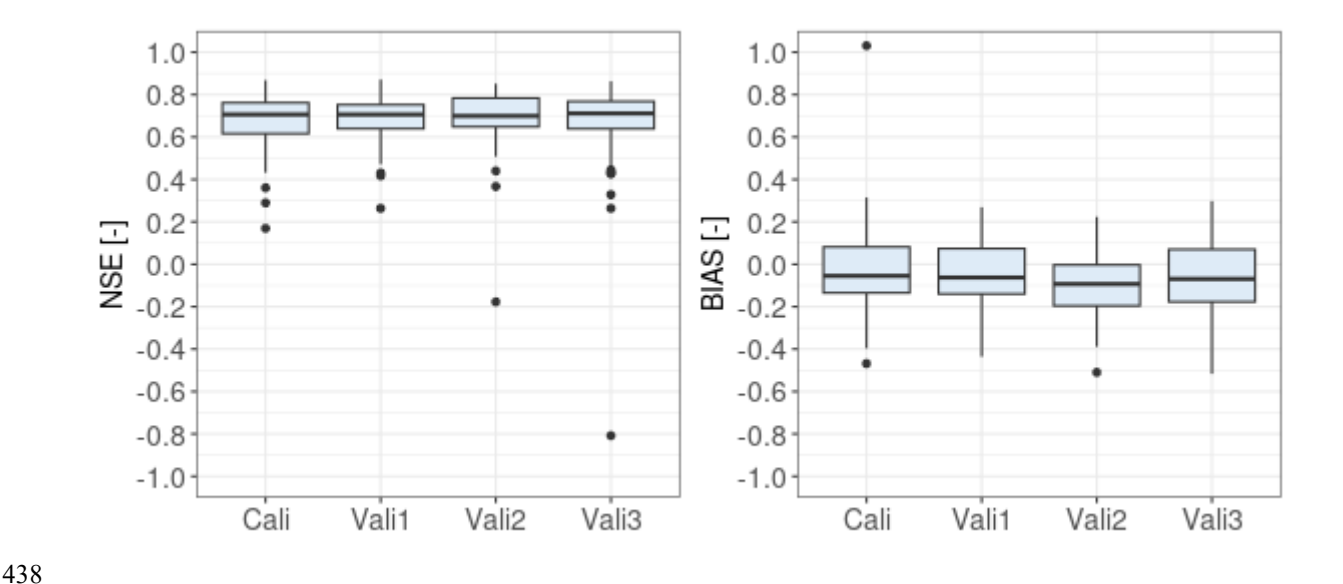


Figure 6: DistHBV model performance in terms of NSE and BIAS for the 85 calibration catchments in the calibration period 2000 – 2007 (Cali), for the 85 calibration catchments in the validation period 2008 – 2014 (Vali1), for the 38 validation catchments in the validation period 2008 – 2014 (Vali2) and for all 123 catchments in the period 1981–2014 (Vali3).

6.2 DEW

Distributed Element Water balance model (DEW) hydrological model (Beldring, 2008; Li et al., 2015) was used to calculate climate change impacts on glaciers and hydrological processes for 12 given glacier regions in Norway. This model differs from distHBV in the respect that it also calculates changes in glacier ice area, volume and surface elevation, and water balance. In addition, the model requires additional information as input, such as ice thickness and glacier area for grid cells with glaciers.

DEW applies a simplified model called DeltaH (Huss et al., 2010) to describe the changes in glacier ice area, volume and surface elevation. The method simulates the impacts of ice movement that transports mass from the highest to the lowest areas of the glacier. Simulations without taking this redistribution of glacier ice into account will give incorrect estimates for both glacier changes and the water flow from the glacier. It is based on historically observed elevation changes of the glacier surface elevation and how these are distributed over the glacier area. The pattern of change is then used when simulating the development of glacier ice area, volume and surface elevation under climate scenarios by having the model redistribute mass over the glacier at the end of each mass balance year. Ice melt caused by negative mass balance results in diminishing of the



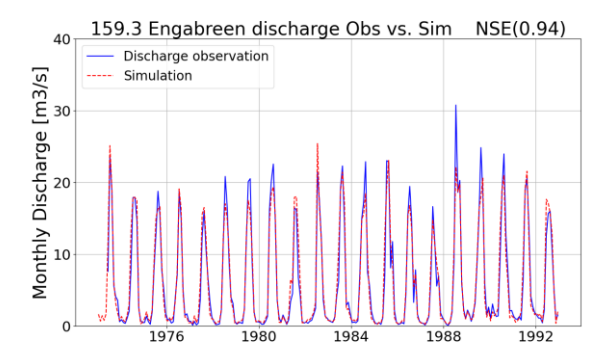


glacier ablation area. Simulations with more advanced, physically based glacier models that simulate the flow of ice in the glaciers would probably be more realistic but are more demanding to run and require much more input data than are not available for most glacier areas in Norway.

Different from the DistHBV model, DEW was calibrated against observed daily streamflow and annual mass balance data for six out of the twelve regions. Within each of the six regions, one optimal model parameter set was determined for all glaciers and catchments. This strategy was chosen to avoid discontinuities in model results between or along catchment boundaries and ice divides. For the remaining six glacier regions where there were no streamflow data available, model parameters were transferred from the nearest glacier region with calibrated parameters. Fixed periods were not used for calibration and validation as in the case of DistHBV, because the availability of observed data varied both in time and space. It was a challenge to find both mass balance and streamflow time series of good quality at the same period, leading to limited time series available for model validation in some cases.

Although the glacier module in DEW is more advanced than in DistHBV, DEW uses a temperature-based degree-day model to estimate potential evapotranspiration, and it uses only daily mean temperature and precipitation as forcing data. Snow and glacier ice melt were calculated using a degree-day model, with different degree-day factors for snow and ice.

DEW was calibrated using the same parameter estimation routine (PEST) as used for distHBV. During model calibration, mean NSE value is 0.75 for daily discharge of 19 gauging stations downstream of the glaciers, and 0.72 for annual mass balance for six glaciers. The mean NSE value for daily discharge during model validation is 0.74. Figure 7 compares the observed and simulated discharge and mass balance for one of the best performing glacierized catchment (Engabreen) as an example. It shows that the model can well reproduce both monthly discharge and annual glacier mass balance with NSE larger than 0.7.



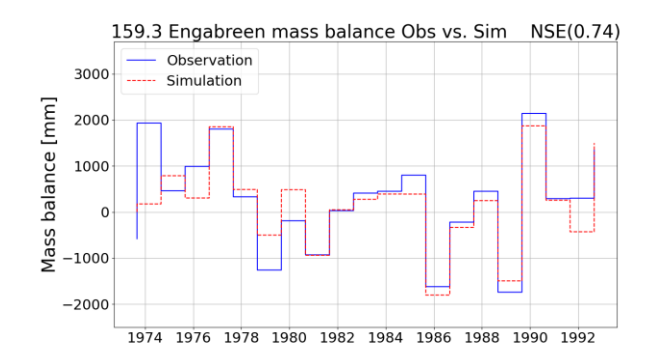


Figure 7: The observed and simulated discharge (left) and annual mass balance (right) for the catchment Engabreen.





7 National climate projections

7.1 Ensemble means and ranges

There are 20 climate projections for mainland Norway at 1km spatial resolution with daily time steps under the RCP4.5 scenario from the COR-BA-2025 dataset. Figure 8 shows 30-year running means of annual temperature and precipitation sums from 1971 to 2098 for Norway. There is a clear increase in temperatures visible in the mean and the whole ensemble. For precipitation, the ensemble mean is also increasing but the lower limit of the projection ensemble is showing a stable precipitation amount of about 1325 mm/year. The observed historical values are mostly within the simulated precipitation and temperature ensembles but are located at the lower end of the ensemble before the year 2000 and at the upper end afterwards, indicating that the RCP4.5 ensemble underestimates recent temperature and precipitation trends in Norway.

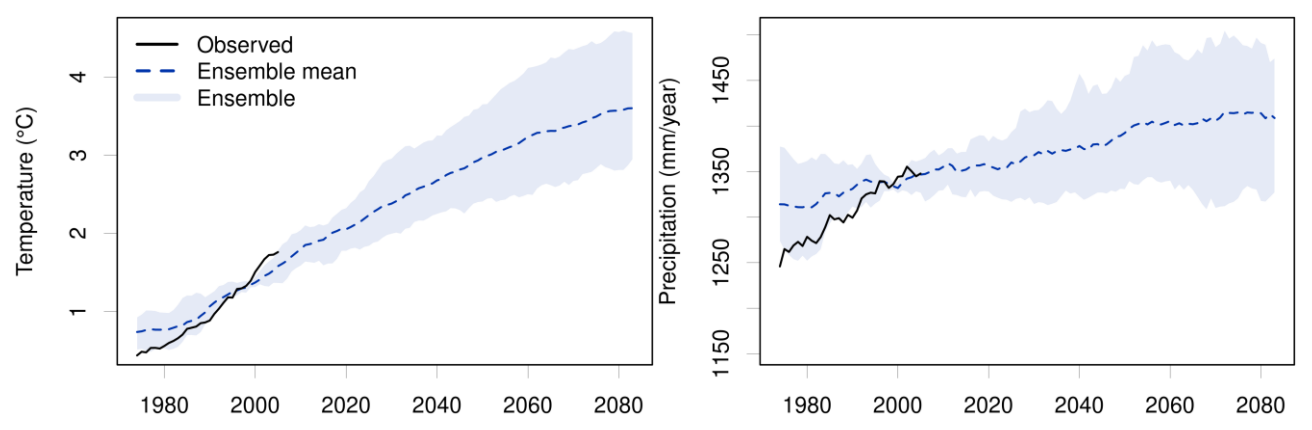


Figure 8: Simulated 30-year running means of temperature (left) and precipitation (right) from the COR-BA-2025 ensemble of 20 climate projections (10 GCM-RCM combinations x 2 bias-adjustment methods) for Norway under the RCP4.5 emission scenario.

Looking at the spatial distribution of changes from the reference period 1991–2020 to the far future period 2071–2100 (Fig. 9), a generally larger increase in temperatures towards the North is apparent, with about one to two °C in the southern and two to three °C in the northern half of Norway. Precipitation is increasing as well with exceptions of some isolated areas along the coast and in the mountains. Generally, the precipitation increases are small and below +12%.





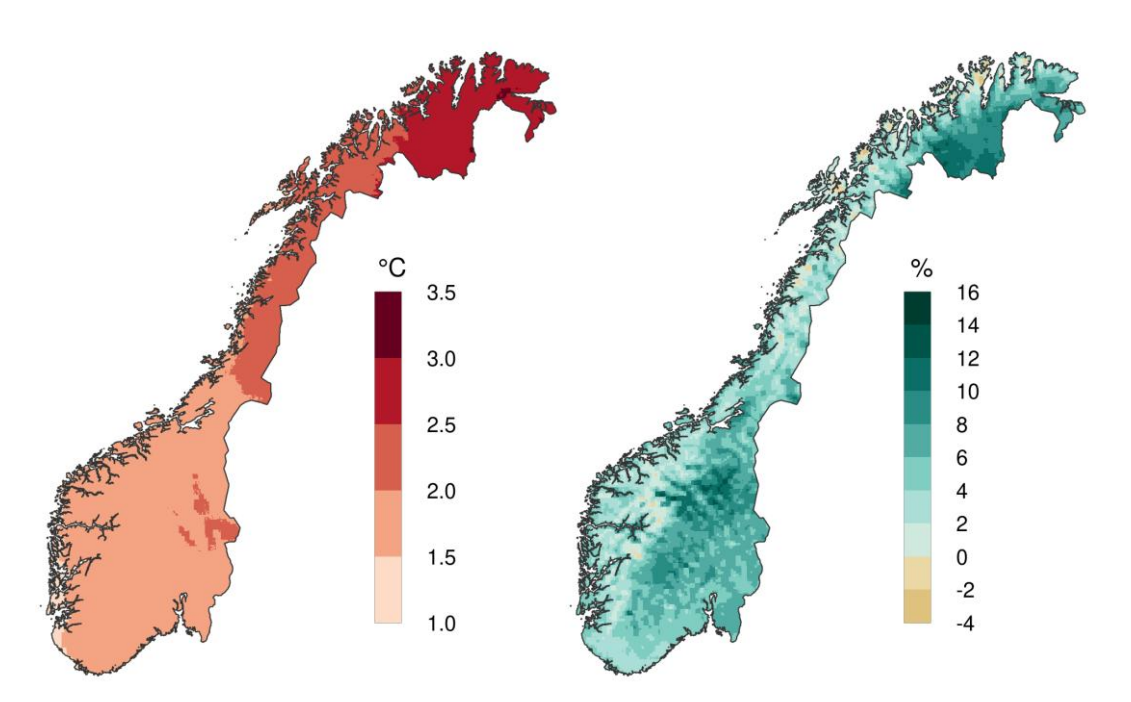


Figure 9: COR-BA-2025 ensemble mean (left) changes in temperature (°C) and (right) relative changes in precipitation (%) in the scenario period 2071–2100 relative to the reference period 1991–2020 under the RCP4.5 scenario for mainland Norway.

7.2 Effects of two bias-adjustment methods

The effects of the two bias-adjustment methods on the preservation and altering of the seasonal climate change signals of the RCMs is shown in Fig. 5 and discussed in Section 5.3.2. Similarly, the two methods have different effects on the monthly climate change signal due to their design. While EQM is designed to preserve the monthly climate change signals, the 3DBC method is designed to provide spatial, temporal and inter-variable structures based on the reference data. However, as can be seen in Fig. 10 and 11, the shapes of the climatologies from EQM and 3DBC are similar and in agreement with the observed ones. As already seen for the seasonal changes (Fig. 5), precipitation and temperature changes in 3DBC are larger than in EQM in winter months (especially January and February) and smaller in spring and summer (April to June) for the far future period (2071–2100). For the near future (2041–2070), the difference in the changes from EQM and 3DBC are less systematic but 3DBC shows a more pronounced increase in autumn precipitation than EQM (Fig, 11). For the current climate (1991–2020), the 3DBC method results in climatologies that are similar for all models and thus a small ensemble-spread compared to the EQM data. This is especially true for precipitation (Fig. 11).



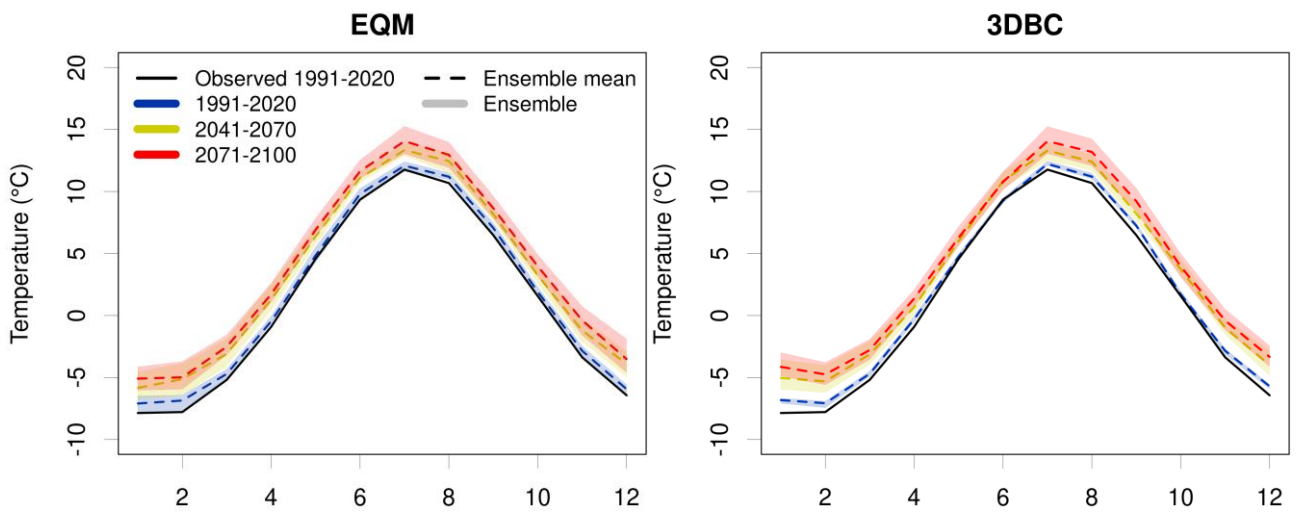


Figure 10: 30-year mean monthly temperatures for Norway for different time periods using the EQM (left) and 3DBC (right) biasadjusted climate projections.

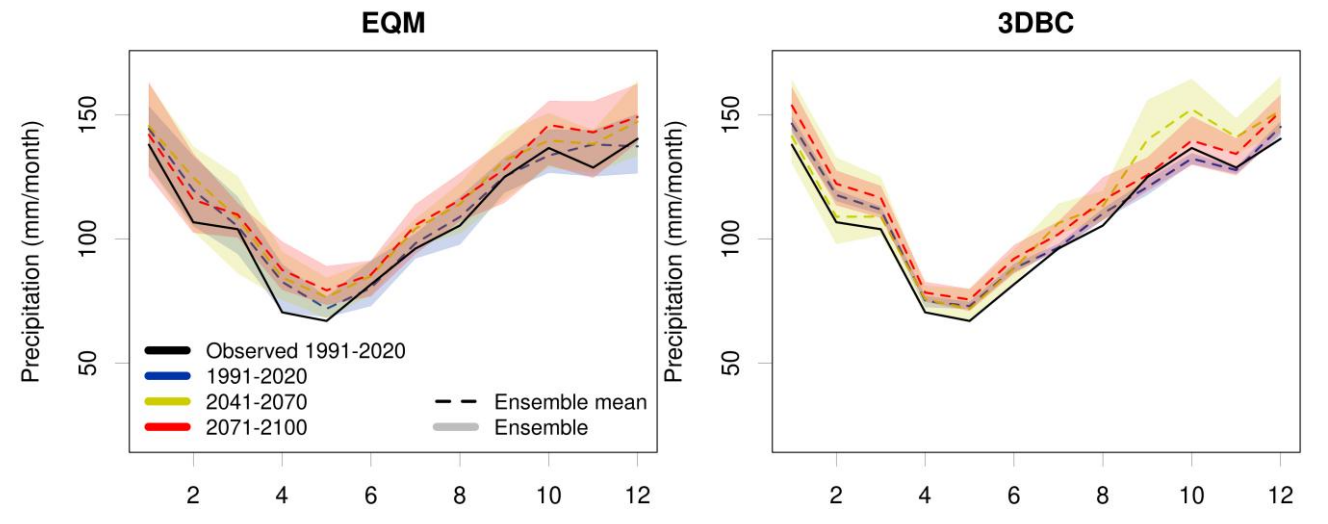


Figure 11: 30-year mean monthly precipitation amounts for Norway for different time periods using the EQM (left) and 3DBC (right) bias-adjusted climate projections.

7.3 Uncertainty analysis

Besides the two different bias-adjustment methods, the various GCM-RCM combinations contribute to uncertainties in the climate projections. In this section, we analyse the contribution of these two uncertainty sources using the ANOVA method (Vetter et al., 2017). Since each GCM is combined with different RCMs (see Section 4), we don't distinguish the GCMs and RCMs as different uncertainty sources here, but consider the GCM-RCM combinations as one uncertainty source. The two bias-adjustment methods are considered the second uncertainty source.





Since our implementation of 3DBC conserves the annual changes from EQM, the annual fraction of variance from the ANOVA analysis (Fig. 12 and 13) is solely dependent on the GCM-RCM combination. On a seasonal scale, the largest contribution to temperature uncertainties still comes from the GCM-RCM combinations. However, for spring and autumn the bias-adjustment contribution can be of similar size, especially in the near future projections. Interactions between the two uncertainty sources are generally small.

For precipitation, the contribution to the overall uncertainty from the bias-adjustment methods is larger than the contribution from the climate models for spring and autumn in the near future. Also for the other two seasons, the different contributions are of similar size for the near future. Interestingly, for the far future, the contribution from the climate models is clearly larger than the contribution from the bias-adjustment methods for all seasons. For precipitation, the interactions are larger than for temperature and can reach magnitudes similar to the single contributions.

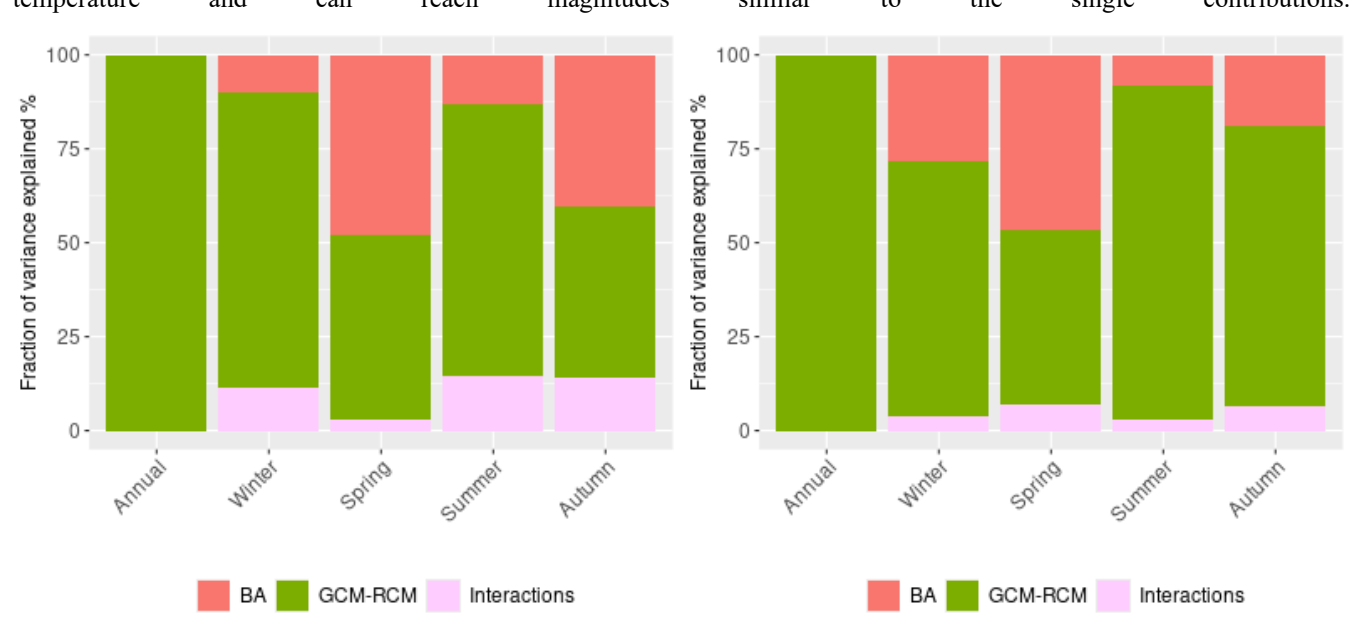


Figure 12: the fraction of variance in projected temperature changes explained by bias-adjustment methods (BA), GCM-RCM combinations and their interactions for the near-future period (2041–2070, left) and far-future period (2071–2100, right).



535



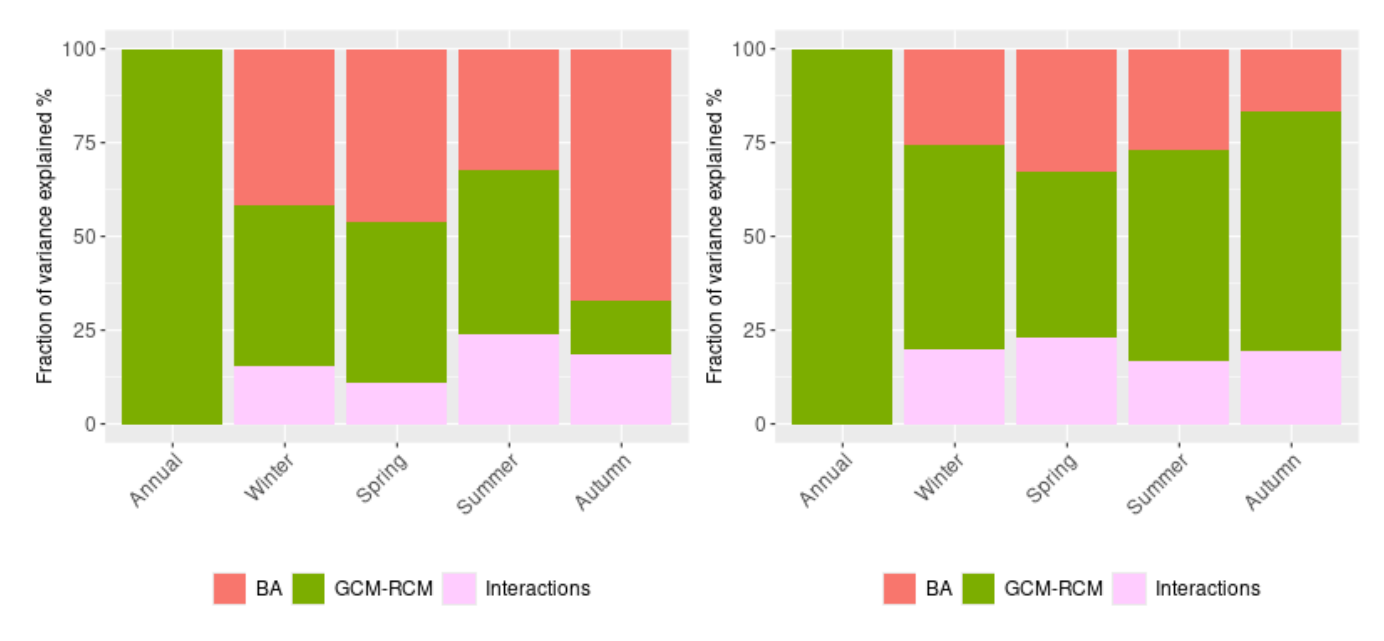


Figure 13: the fraction of variance in projected precipitation changes explained by bias-adjusted methods (BA), GCM-RCM combinations and their interactions for the near-future period (2041–2070, left) and far-future period (2071–2100, right).





8 National hydrological projections

8.1 Ensemble means and ranges

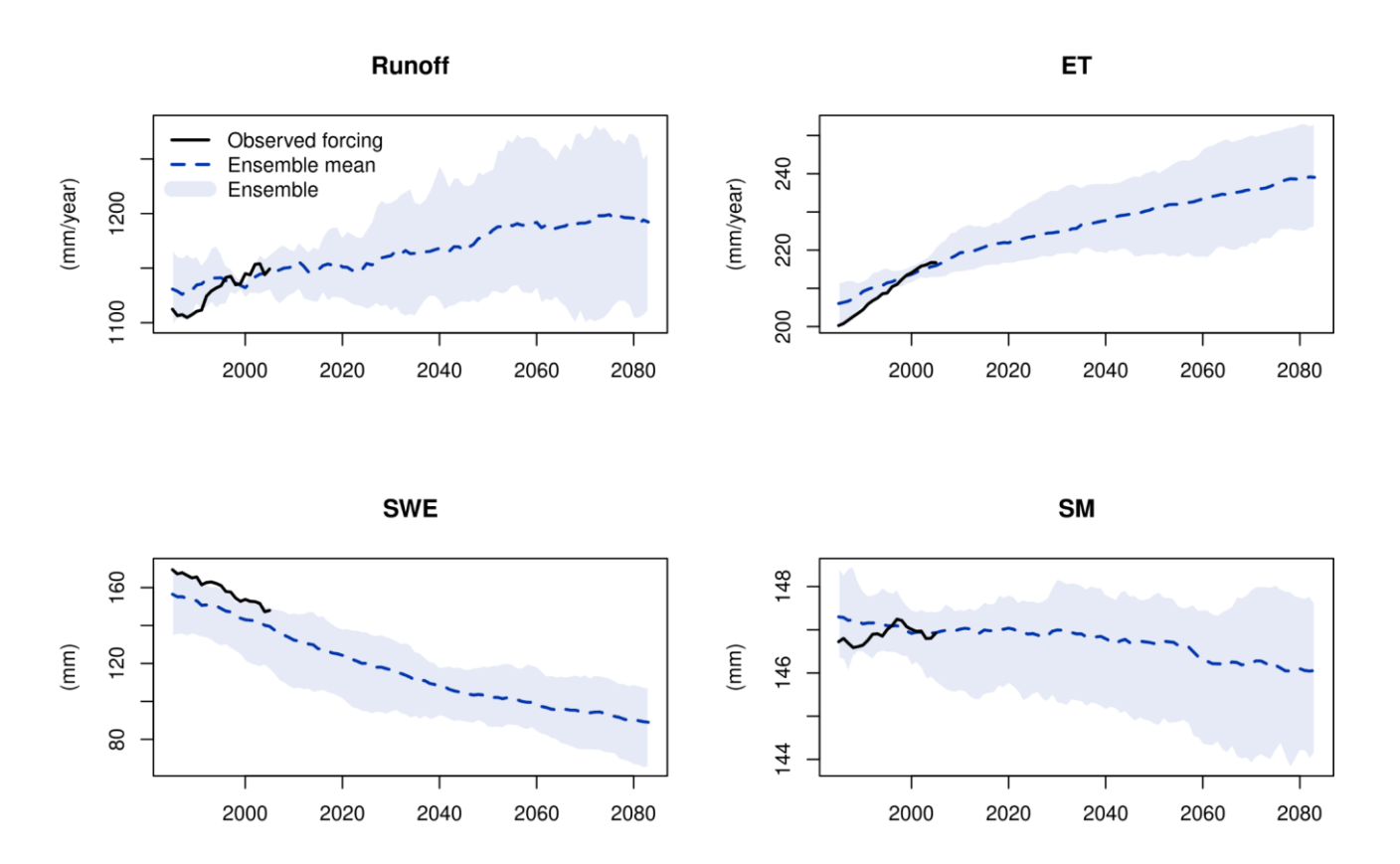


Figure 14: Simulated 30-year running means of annual runoff, evaporation (ET), mean snow water equivalent (SWE) and mean soil moisture (SM) driven by the ensemble of 20 climate projections (10 GCM-RCMs x 2 bias correction methods) under the RCP4.5 scenario. The black line is the simulated water components driven by the observed forcing data.

There are 20 hydrological projections for mainland Norway at 1km spatial resolution with daily time steps under the RCP4.5 scenario from the distHBV-COR-BA-2025 dataset. Figure 14 shows the projected annual sum/mean of these variables from 1971 to 2098 for mainland Norway. Both the ensemble means of runoff and evaporation have an increasing trend while the ensemble means of snow water equivalent and soil moisture trend to decrease towards the end of this century. The simulated runoff, evaporation, and soil moisture driven by the seNorge forcing data (black lines) are generally within the boundary of the 20 simulations in the historical period, and they have a good agreement with the ensemble mean after the year 2000, indicating good estimates of these variables driven by the bias-adjusted climate projections. However, all snow water equivalent simulations are generally underestimated compared with the simulated snow water equivalent driven by the seNorge



551

552

553

554

555

556 557

558

559

560

561

562



550 data, indicating that snow generation is not well reproduced. It is mainly due to inaccurate inter-variable, spatial and temporal dependence between the bias-adjusted atmospheric variables when only the EQM method is used (see section 8.2).

Figure 15 shows the spatial distribution of the ensemble mean changes in the last scenario period (2071–2100) relative to the reference period (1991–2020). In general, the increasing changes in runoff are dominant in the whole country, except glacier retreat areas around the glaciers and the coastal areas in the northern part of Norway. The increasing changes are minor (<5%) or moderate (5–10%) in most parts of the country and strong increase in runoff (> 10%) occurs mainly in the glacier areas, lakes and rivers as well as some northernmost areas. Due to the warmer and wetter climate in the future, evaporation is projected to increase in the whole country, especially in western and central Norway. In contrast, the annual mean snow water equivalent will decrease in the whole country in the far future, with a strong decrease (<-75%) along the coast. Note that snow volumes along the coast of Southern Norway are small in today's climate. The absolute decrease in annual mean snow water equivalent is not stronger along the coast than mountainous areas. Soil moisture will decrease in most parts of the country due to the increase in evaporation, and moderate to strong decreases (<-5%) are mainly found in some southern areas and the coastal regions in the north.



565

566

567

568569



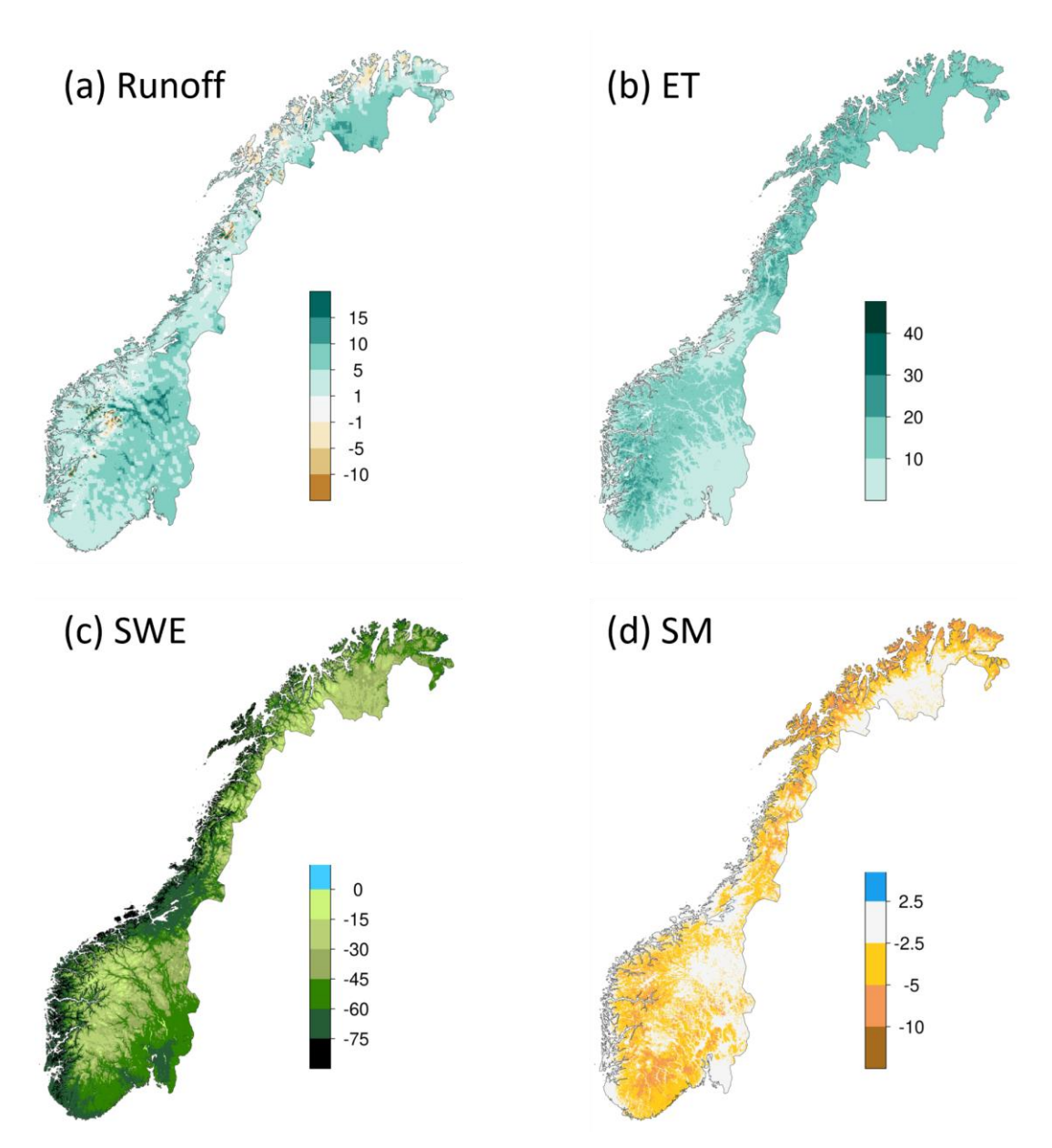


Figure 15: ensemble mean changes (%) in annual runoff (a), evaporation (ET) (b), snow water equivalent (SWE) (c) and soil moisture (SM) (d) in the scenario period 2071–2100 relative to the reference period 1991–2020 under the RCP4.5 scenario for mainland Norway.

8.2 Effects of the two bias-adjustment methods

In this section, we provide a general overview of the effects of the bias-adjustment methods on hydrological projections. Figure 16 shows the seasonal relative changes in runoff including all 20 projections, 10 projections using the EQM bias-adjustment





method and 10 projections using the 3DBC method, respectively. The results show that there is a neglectable difference in annual changes between the bias-adjustment methods. However, the bias-adjustment methods lead to different seasonal runoff changes and their effects vary in scenario periods and seasons. In the near future, the largest difference in the ensemble median changes between the bias-adjustment methods is found in autumn (ca. 13%), followed by the difference in spring (ca. 8%), winter (ca. 5%) and summer (ca. 3%). The 3DBC method leads to higher runoff changes in winter and autumn, but lower runoff changes in spring and summer than the EQM method. As a result, the two methods lead to similar changes in annual changes. In the far future, the bias-adjustment methods mainly affect the runoff changes in winter and spring, resulting in a difference in median changes of 12% in winter and 5% in spring. There is almost no difference in median runoff changes between the methods in summer and autumn. These results indicate that the two bias-adjusted methods mainly affect the snow accumulation and melt processes, which occur in autumn, winter and spring in the near future and in winter and spring in the far future. In addition, 3DBC always leads to higher runoff in winter and lower runoff in spring than EQM in both scenario periods.

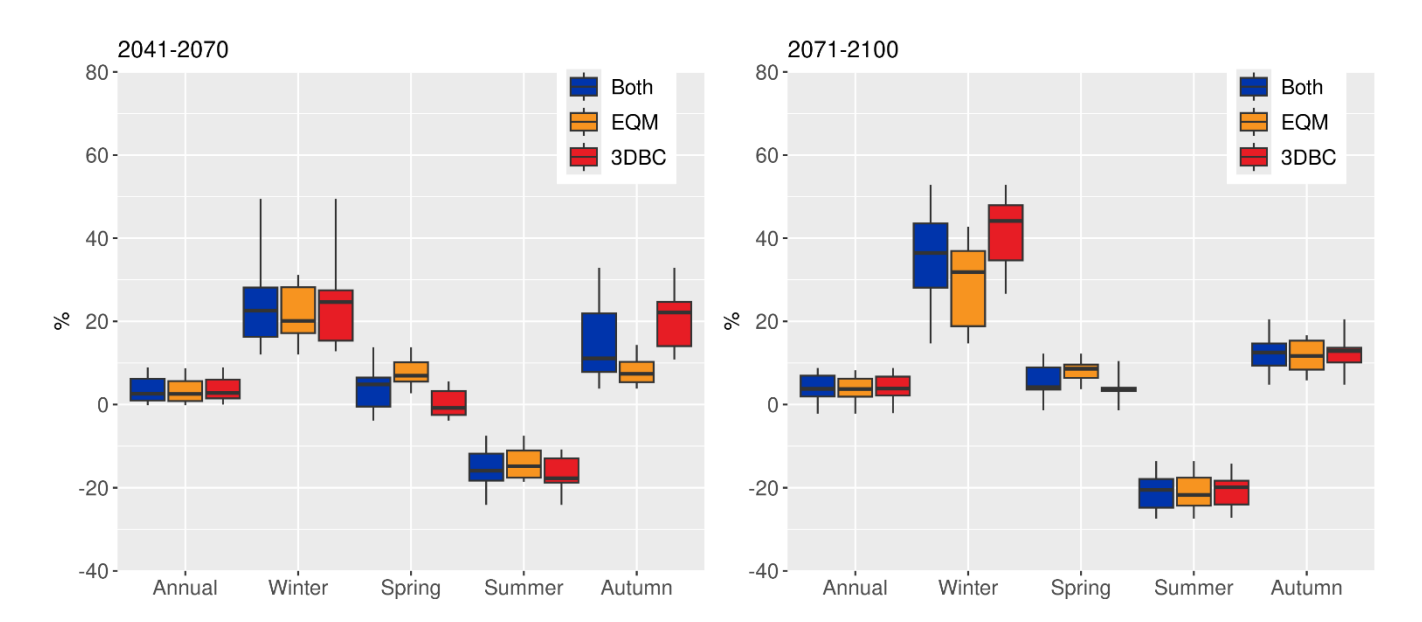


Figure 16: relative changes in runoff for different seasons in the scenario periods 2041–2070 (left) and 2071–2100 (right) relative to the reference period 1991–2020 under the RCP4.5 scenario for mainland Norway.





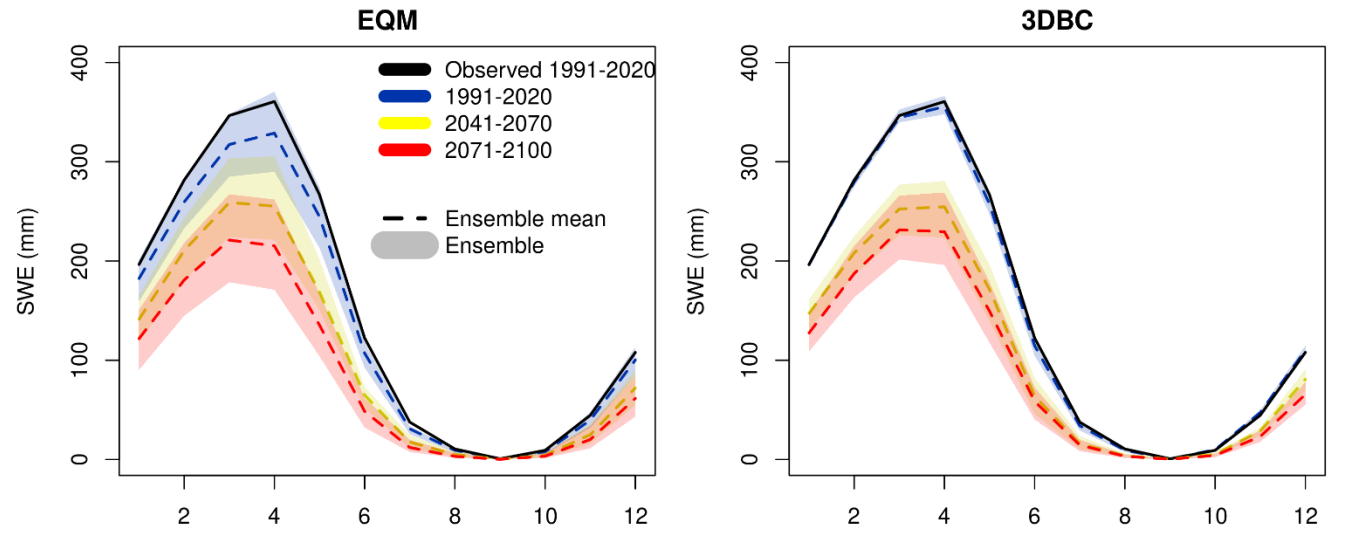


Figure 17: Simulated monthly snow water equivalent (SWE) for mainland Norway using the EQM (left) and 3DBC (right) bias-adjusted climate projections. Black line: the simulated SWE using observed forcing data in 1991–2020. Blue, yellow and red dash lines: the ensemble mean of simulated SWE in different periods, while the blue, yellow and red areas include the ensemble of 10 projections.

In order to illustrate the effects of the two bias-adjustment methods on snow processes, we compared the monthly snow water equivalent in the historical and scenario periods driven by different bias-adjusted projections as well as the ones driven by the observed forcing data (Fig. 17). In the historical period, the ensemble mean of monthly snow water equivalent driven by the 3DBC bias-adjusted projections agrees well with the simulated one driven by the observed forcing data. The EQM bias-adjusted simulations generally lead to underestimation of monthly snow water equivalent, especially in March and April, similar to the findings by Meyer et al. (2019). In addition, the historical snow simulations using the EQM method vary substantially between climate models, while all bias-adjusted climate projections using the 3DBC method lead to similar monthly SWE, indicating more robust snow projections in the historical period using the 3DBC method than the EQM method.

The two bias-adjusted methods also affect the projected changes in snow water equivalent in the scenario periods, especially in the near future. The ensemble mean of monthly snow projections using the 3DBC methods show average decreases of about 44 and 55 mm/month in the near and far future periods relative to the reference period respectively, while the ensemble mean using the EQM method decreases by 33 and 50 mm/month on average in the near and far future periods, respectively. It is due to higher snow water equivalent in the historical period and lower snow water equivalent in the near future using the 3DBC bias-adjusted projections than those using the EQM projections. However, the differences in snow water equivalent between the near and far-future periods are smaller using the 3DBC than the EQM method, leading to closer agreement on snow water equivalent changes in the far future between the two methods. The uncertainty bounds of snow projections using the 3DBC





method are still smaller than the uncertainty bounds using the EQM method in both future periods, but the differences in uncertainty bounds between the two methods is less substantial than the ones in the historical period.

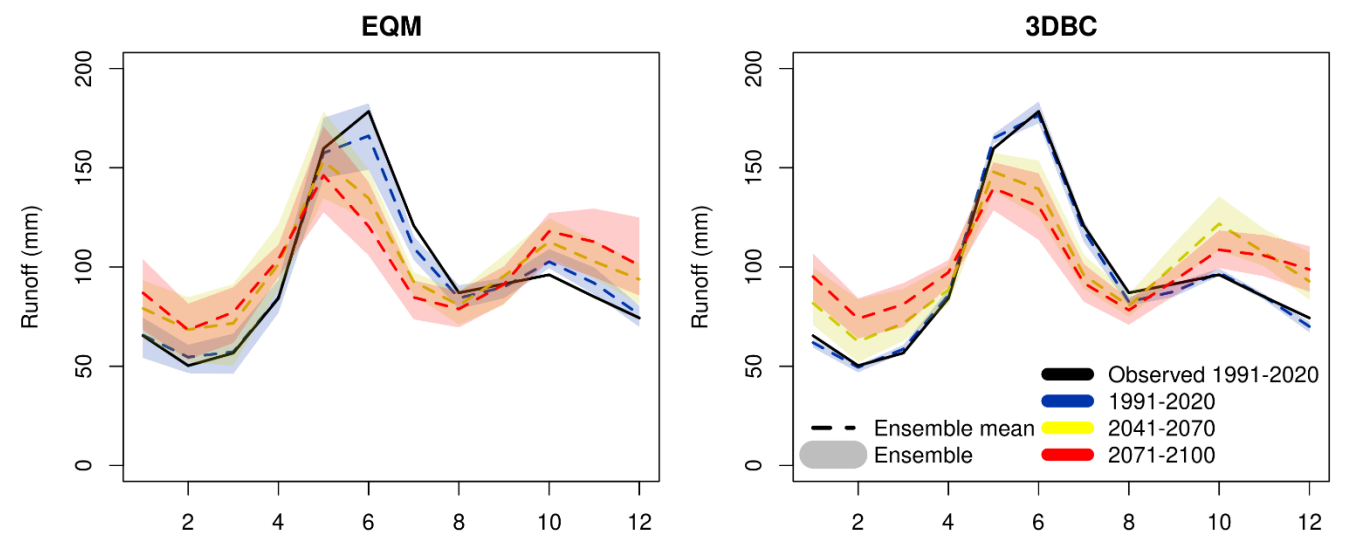


Figure 18: Simulated monthly runoff for mainland Norway using the EQM and 3DBC bias-adjusted climate projections. Black line: the simulated runoff using observed forcing data in 1991–2020. Blue, yellow and red dash lines: the ensemble mean of simulated runoff in different periods, while the blue, yellow and red areas include the ensemble of 10 projections.

Partly due to different snow simulations, the monthly runoff projections also differ between the two bias-adjustment methods (Fig. 18). In the historical period, the simulated runoff using the 3DBC bias-adjusted climate simulations also agrees well with the simulated runoff using observed forcing data, while the simulations using the EQM bias-adjusted climate simulations underestimate runoff from June to July that is generated by snow melt, mainly due to less snow storage in winter and spring (Fig. 17). There is also an overestimate of runoff from October to November using the EQM bias-adjusted climate simulations, indicating that other hydrological processes besides snow are also affected by the inaccurate spatial and temporal correlations of climate variables. Similarly, the runoff simulations using the EQM bias-adjusted climate projections have larger uncertainty bounds than the ones using the 3DBC projections.

In the future periods, the runoff projections using the 3DBC method show larger increase and decrease in monthly changes relative to the historical period than using the EQM ones. In addition, the 3DBC bias-adjusted climate projections lead to higher runoff in autumn in the near-future than in the far-future while the EQM projections show contradicting changes. Different from the snow projection uncertainty, the runoff uncertainty using the 3DBC method is not always smaller than the one using the EQM method in all months. In addition, the large runoff uncertainty in the historical and future periods does not lead to large uncertainty of runoff changes. As shown in Fig. 16, the uncertainty bounds of runoff changes using the 3DBC method is not substantially larger than the uncertainty of changes using the EQM method.





8.3 Uncertainty analysis

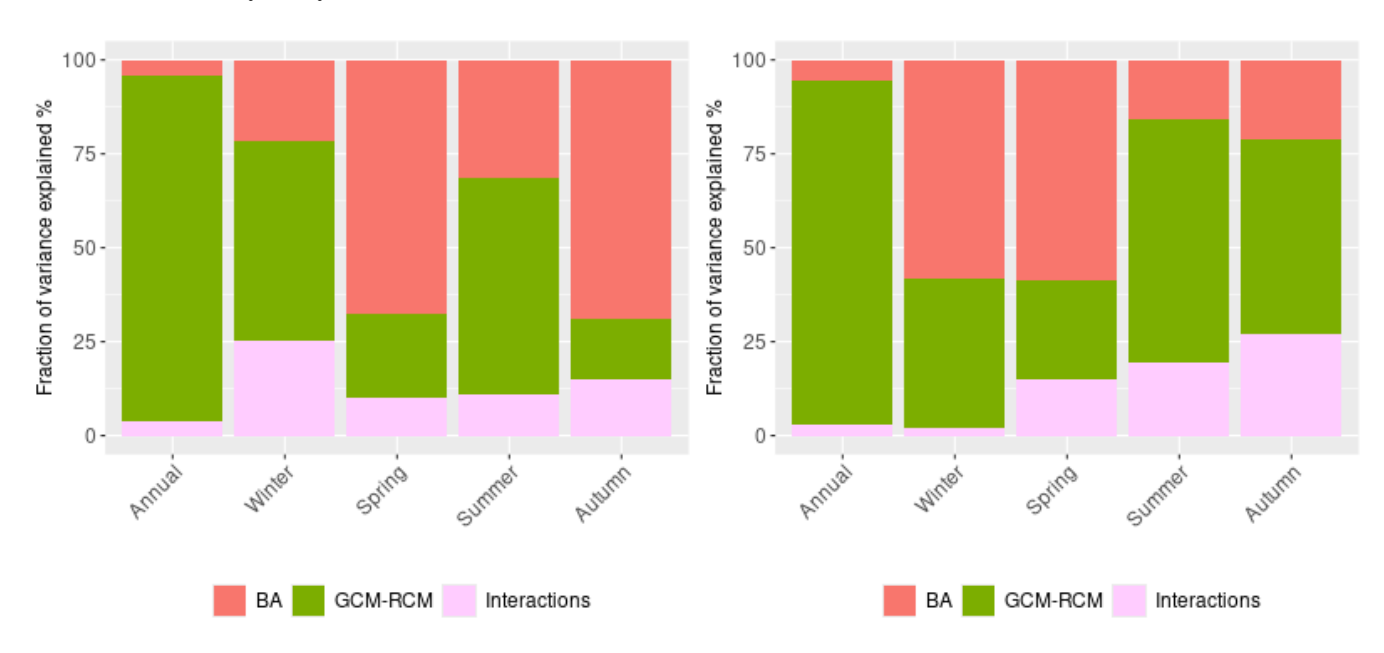


Figure 19: the fraction of variance in runoff change projections explained by bias-adjustment methods (BA), GCM-RCM combinations and their interactions for the near-future period (2041-2070) (left) and far-future period (2071-2100).

Similar to temperature and precipitation, we assessed the contribution of the two bias-adjustment methods and GCM-RCM combinations to the uncertainty in the runoff projections. Figure 19 shows the fraction of variance from the ANOVA analysis for the GCM-RCM combinations, bias-adjustment methods and their interactions for the two future periods. For both periods, it is obvious that the climate model combinations contribute to the majority of the annual runoff change variance (> 90%). However, the bias-adjustment methods play important roles in the seasonal runoff changes, especially in spring and autumn in the near future and in the winter and spring in the far future, explaining more than 50% of the runoff change variance. For summer, the climate model combinations are always the major uncertainty source, explaining more than 50% of the total runoff change variance. These results highlight the effects of bias-adjustment methods on seasonal runoff change projections.

9 Discussion

9.1 Limitations of the methodology

In this study, we present the whole modelling chain that produces the updated national ensembles of climate and hydrological projections for the new Climate in Norway report CiN-2025. This modelling chain includes selection of emission scenarios and climate models, downscaling and bias-adjustment methods and hydrological models. Although we have made a number





of substantial improvements in each component of the modelling chain, there are still limitations and weaknesses in the methodology, which require further development for future climate impact assessments.

The first component in the modelling chain is to select appropriate emission scenarios and climate projections from a large ensemble of GCM and RCM outputs manageable throughout the complete chain. As a national climate assessment report following the sixth IPCC report, it would have been ideal to apply the most updated emission scenarios (i.e., the SSPs) and the corresponding climate projections. However, due to the long time needed to make the newest RCM results available within the CORDEX framework and the time limit of the national report, we had to apply the climate projections corresponding to the fifth IPCC report for the low- and median emission scenarios (RCP scenarios). Complements of the national climate projections for SSP emission scenarios are expected in the future to provide up-to-date knowledge on climate change impacts.

Since the EURO-CORDEX ensemble for the RCP scenarios is now much larger than for CiN-2015, the climate projections for CiN-2025 are more representative of the full range of climate changes ensembles. However, the restriction to ten models per scenario stemming from the complete modelling chain still partly limits the representativeness of the full possible outcome and model variability. In CiN-2025, this limitation is taken into account for temperature and precipitation using empirical-statistical downscaling results from the complete set of available GCMs, which is not shown in this study. Additionally, RCMs are still subject to general limitations of model simplifications, such as internal parameterizations and spatial resolution. Further, some technical limitations remain in the RCM outputs, for example, some models provide outputs for 360 days per year, no leap year days or start in 1970 and end in 2098. This brings challenges for impact models and requires pre-processing before bias-adjustment. In addition, the historical period simulated by the RCMs does not cover the current standard normal period (1991–2020). This is a drawback since it is easier for the general public to compare the climate change signals with respect to the climate normal than other non-standard periods (e.g., 1976–2005). Although the use of the first few years from the scenario projections as reference period is not optimal, and the choice of the reference period can lead to different climate changes signals (Liersch et al., 2020), the use of the most recent standard normal period improves the public acceptance and understandability substantially, which is most important for the target users of a national report such as CiN-2025.

As the second component of the modelling chain, downscaling and bias-adjustment methods allow presenting projected climate and hydrological changes at a spatial resolution of 1x1 km for the complex topography of Norway. Providing such high resolution data needs high computational costs and makes it challenging to test and apply a large number of bias-adjustment methods. Hence, we only selected EQM as the bias-adjustment method as it is robust for different climatological regimes and well established. The 3DBC method is further applied on the EQM bias-adjusted variables to improve the inter-variable, spatial and temporal dependencies. This multivariate bias-adjustment method indeed improves the hydrological projections, especially for snow simulations, and reduces the uncertainty range, especially in the reference period. However, the 3DBC method (Section 5.2) leads to different climate change signals compared to the original RCM signals on sub-annual scales





because it imposes temporal dependency structures on the future projections similar to the ones from the reference datasets. This may be considered a weakness of the approach and more evaluation and development of multivariate bias-adjustment methods are required to further improve the existing methods. As discussed in François et al. (2020), the choice of method may differ from case to case, depending on which statistical properties from the RCMs need to be preserved or corrected. Based on our findings, users of the bias-adjusted data may select the appropriate dataset depending on their needs, or simply consider the two methods being equal, resulting in a broader ensemble.

Regarding hydrological models, both the potential evaporation module and glacier modelling have been improved compared to the model used in CiN-2015. The Penman-Monteith method substantially improves the spatial distribution of evaporation estimates under climate scenarios by considering more climate variables and representing different land cover types, while the dynamic glacier modelling by DEW successfully avoids unrealistically high runoff from the glacier retreat areas under a warming climate. However, the simulations of DistHBV may still suffer equifinality problems due to a large number of calibration parameters, which do not represent the physical characteristics of specific land use and soil types. In addition, we reclassify the soil types into five major groups in order to reduce the number of calibration parameters related to soil processes. This may lead to unreliable simulations for the areas where the soil condition is largely different from the major soil types. Therefore, both the calibration procedure and the spatial representation of soil physical characteristics are expected to improve in the future national applications. The emerging machine learning techniques have been successfully used to calibrate one distributed land surface model (Farahani et al., 2025), and they are expected to play more important roles in hydrological model calibrations.

Last but not least, vegetation types and characteristics are static in our hydrological modelling under climate change scenarios, but the changes in vegetation characteristics are expected under a warming climate. Huang et al. (2025) assessed the effects of forest growth and forest management on water resources in six Norwegian catchments under the RCP2.6 and RCP4.5 emission scenarios. They found that forest growth would offset the increase in runoff in the catchments, where the deciduous forest is dominant. It implies that the runoff in the deciduous forest areas, especially in North Norway, may be overestimated in our present runoff projections. For the next generation CiN report, the land use and vegetation change scenarios should be included in the hydrological modelling if such scenarios are available.

9.2 Application

Despite the limitations mentioned above, the COR-BA-2025 and distHBV-COR-BA-2025 datasets generated by the presented modelling chain provide the most updated, comprehensive and detailed hydrometeorological projections for mainland Norway. These national projections serve as the scientific basis for research on climate change impacts in Norway. The gridded hydrometeorological projections from CiN-2015 have already been used to derive new indices for specific application, e.g. snow-dependent tourism (Kuya et al., 2024; Mayer et al., 2023), reindeer husbandry (Hanssen-Bauer et al., 2022), frost decay





exposure on building projects (Gaarder et al., 2024) and road maintenance (Nilsen et al., 2021). In addition to impact modellers, who represent an advanced user group, NCCS aims at providing tailored information for practical climate adaptation. Products derived from the national projections have also been widely used in local planning, mainly because government guidelines (Norwegian Government, 2024) required municipalities to take climate change into account in planning. Climate factsheets (Hisdal et al., 2021) provided the most relevant information to guide the climate adaptation work, and were pointed out as a core reference in government guidelines. See Nilsen et al. (2022) for an overview of the steps from climate model output to actionable climate information.

Besides the possibility to update existing applications that used the gridded dataset from CiN-2015, COR-BA-2025 and distHBV-COR-BA-2025 provide additional variables, such as wind speed, pressure, evaporation, radiation and relative humidity. This improves the utility of the dataset for e.g., ecological modelling (see Pirk et al., 2023 for an example). It is expected that the new dataset will facilitate use in an even wider range of applications in the coming years, for climate change impacts on e.g., glaciers, drought, landslides and water availability. Further work will involve user groups such as municipal planners to co-create climate services based on the hydrometeorological projections presented.

Finally, we should note that the gridded datasets distHBV-COR-BA-2025 are not designed to use for flood indices, or climate change allowances for floods because distHBV was calibrated against many catchments simultaneously. Instead, the outputs from specific flood models should be used (Lawrence, 2020; Carr et al., 2023). The flood models include two lumped hydrological models and were calibrated against observed discharges for each catchment separately. Hence, the flood models produce more reliable estimates of high (and low) flow for specific catchments.

10 Conclusions

In this study, we present the whole modelling chain behind the production of updated national ensembles of climate and hydrological projections for the official "Climate in Norway" assessment report. We also provide insight into the hydrometeorological projections, which we termed COR-BA-2025 (standing for CORDEX-Bias Adjusted, updated in 2025) for climate projections and distHBV-COR-BA-2025 for hydrological projections, and analyse their uncertainties. The modelling chain (Fig. 2) includes the selection of GCM-RCM combinations for Norway from a large ensemble of EURO-CORDEX simulations, the application of two bias-adjustment methods and distributed hydrological modelling including a physically-based potential evaporation approach and a dynamic glacier model. Compared to the previous national assessment report, the new climate projections are considered more representative for Norway due to a larger ensemble of EURO-CORDEX simulations taken into account and a systematic analysis of the projections.

A multivariate bias-adjustment method has been applied for the first time over the whole of Norway for the complete atmospheric dataset consisting of nine variables. This new method leads to more consistent data in space, time and between



737

738

739

740

741

742

743

744

745

746747

748

749

750

751

752

753

754

755

756

757

758

759

760

762

(Dobler, 2025).



variables, and to more robust hydrological simulations than the univariate empirical quantile mapping method (especially for snow and in the reference period), but it does not preserve climate change signals on a sub-annual scale. However, the uncertainty ranges of runoff change projections are not significantly different between the two bias-adjustment methods, especially at the annual scale. An uncertainty analysis shows that the climate projections are the major source of uncertainty for annual runoff change, while the selection of the bias-adjustment method plays an important role on seasonal changes. Despite the advancement in the presented methodologies and modelling chain, there is still room for further improvement in future climate impact assessment studies. Currently we foresee that additional emission scenarios and GCM-RCM combinations from the EURO-CORDEX initiative will be evaluated and the bias-adjustment methods will be further developed to overcome the current limitations. In addition, the calibration procedure and the calibration parameters in the hydrological modelling will be further improved using advanced machine learning techniques. If possible, the land use and vegetation changes scenarios should also be considered in hydrological modelling. The methodological description provided here serves as core knowledge for any further application of the gridded products, which are expected to be used in a wide range of climate impact assessments and development of climate adaptation strategies in Norway. We have thrived to meet the FAIR principles (Wilkinson et al., 2016) for data management. Thus, the complete COR-BA-2025 and distHBV-COR-BA-2025 datasets (Wong et al. 2025) are findable and accessible through the Arctic Data Centre (adc.met.no) at https://doi.org/10.21343/0k90-6w67. The data is stored in NetCDF format following the attribute convention for data discovery (ACDD version 1-3, https://wiki.esipfed.org/Attribute Convention for Data Discovery 1-3) and the climate and forecast metadata conventions (CF version 1.10, Eaton et al., 2022). The code and data are reusable, being open source with non-restrictive licenses. Code availability The code of DistHBV is available at https://doi.org/10.5281/zenodo.17531118 (Beldring, 2025a) The code of DEW is available at https://doi.org/10.5281/zenodo.17530242, (Beldring, 2025b) The R source code of the 3DBC implementation used in this work is available at https://doi.org/10.5281/zenodo.15260334

FQM implementation used the functions *fitQmapQUANT* and *doQmapQUANT* from *R* package *qmap* which is available at

https://doi.org/10.32614/CRAN.package.qmap (Gudmundsson, 2025).



Data availability

763

768

774

775

776



- The **COR-BA-2025** and **distHBV-COR-BA-2025** bias-adjusted daily high-resolution climate and hydrological projections for Norway are freely available at the Arctic Data Centre (<u>adc.met.no</u>) under https://doi.org/10.21343/0k90-6w67 (Wong et al., 2025).
- The reference datasets used in the modelling chain are available at https://doi.org/10.21343/gbq0-4t97 (Huang et al., 2025).

Author contribution

- 769 SM, SLS, TL, WKW and AD performed the analysis of climate model selections and collected the RCM data. WKW and AD
- designed the bias-adjustment experiments and methods and carried them out. IH modified the model code DistHBV and IH
- and SH performed the simulations. SB and KM developed the model code DEW, designed the experiments of DEW and GR
- 772 performed the simulations. SH prepared the manuscript with contributions from all co-authors. AVD, HOH, IBN and SJB
- coordinated the whole project.

Competing interests

The authors declare that they have no conflict of interest.

Acknowledgement

- 777 We acknowledge the World Climate Research Programme, the CORDEX Science Advisory Team (SAT) coordinating body
- of CORDEX, and the Working Group on Coupled Modelling (WGCM) responsible panel for CMIP5 and CMIP6. We thank
- the CORDEX climate modeling groups (listed in Table 1) for producing and making available their model output, CMIP5 for
- 780 providing the driving data, the Earth System Grid Federation (ESGF) for providing access, and the multiple funding agencies
- 781 who support CORDEX, CMIP and ESGF.

782 Financial support

- 783 This article was funded by the Norwegian Centre for Climate Services, and thus supported by the Norwegian Environment
- 784 Agency and the Ministry of Climate and Environment in addition to in-kind contributions from the Norwegian Water
- Resources and Energy Directorate, NORCE and the Norwegian Meteorological Institute.





786 **References**

- 787 Ahlstrøm, A., Bjørkelo, K., and Frydenlund, J.: AR5 klassifikasjonssystem klassifikasjon av arealressurser, Skog og
- 788 landskap, rapport nr. 6/2014, 38 pp. http://hdl.handle.net/11250/2440173, 2014.
- Alifu, H., Hirabayashi, Y., Imada, Y., and Shiogama, H.: Enhancement of river flooding due to global warming, Sci Rep, 12,
- 790 20687, https://doi.org/10.1038/s41598-022-25182-6, 2022.
- 791 Andreassen, L. M., Huss, M., Melvold, K., Elvehøy, H. og Winsvold, S. H.:. Ice thickness measurements and volume
- 792 estimates for glaciers in Norway. *Journal of Glaciology*, 61(228), 763-775. https://doi.org/10.3189/2015JoG14J161, 2015.
- Ayar, P. V., Vrac, M., Bastin, S., Carreau, J., Déqué, M., and Gallardo, C.: Intercomparison of statistical and dynamical
- downscaling models under the EURO- and MED-CORDEX initiative framework: present climate evaluations, Clim Dyn, 46,
- 795 1301–1329, https://doi.org/10.1007/s00382-015-2647-5, 2016.
- 796 Beck, H. E., Zimmermann, N. E., McVicar, T. R., Vergopolan, N., Berg, A., and Wood, E. F.: Present and future Köppen-
- 797 Geiger climate classification maps at 1-km resolution, Sci Data, 5, 180214, https://doi.org/10.1038/sdata.2018.214, 2018.
- 798 Beldring, S.: Distributed element water balance model system. Norwegian Water Resources and Energy Directorate, Report
- 799 no. 4/2008, 40 pp. https://publikasjoner.nve.no/report/2008/report/2008_04.pdf
- https://github.com/DistributedElementWaterModel/Version 3.03, 2008.
- 801 Beldring, S.: nve-sbe/DistributedHby: v 1 (v 1), Zenodo, https://doi.org/10.5281/zenodo.17531118, 2025a.
- Beldring, S.: DistributedElementWaterModel/Version 3.03: v 1 (v 1), Zenodo, https://doi.org/10.5281/zenodo.17530242,
- 803 2025b.
- 804 Beldring, S., Engeland, K., Holmqvist, E., Pedersen, A.I., Ruan, G., Veie, C.A. and Cabrol, J.: Avrenningskart for Norge 1991–
- 805 2020. NVE rapport nr. 36/2022, https://publikasjoner.nve.no/rapport/2022/rapport2022 36.pdf, 2022.
- Beldring, S., Engeland, K., Roald, L. A., Sælthun, N. R., and Voksø, A.: Estimation of parameters in a distributed precipitation-
- runoff model for Norway, Hydrology and Earth System Sciences, 7, 304–316, https://doi.org/10.5194/hess-7-304-2003, 2003.
- 808 Bergström, S.: The HBV model. V.P. Singh (Ed.), Computer Models of Watershed Hydrology, Water resources publications,
- 809 pp. 443-476, 1995.
- 810 Bremnes, J. B.: Probabilistic wind power forecasts using local quantile regression, Wind Energy, 7, 47-54,
- 811 https://doi.org/10.1002/we.107, 2004.





- Bright, R. M., Eisner, S., Lund, M. T., Majasalmi, T., Myhre, G., and Astrup, R.: Inferring Surface Albedo Prediction Error
- Linked to Forest Structure at High Latitudes, Journal of Geophysical Research: Atmospheres, 123, 4910-4925,
- 814 https://doi.org/10.1029/2018JD028293, 2018.
- 815 Carr, S., Lawrence, D., Skaugen, T., and Wong, W. K.: Projected future changes in peak flows and implications for climate
- 816 change allowances, NVE report nr. 26/2023, The Norwegian Water Resources and Energy Directorate, Oslo, Norway,
- https://publikasjoner.nve.no/rapport/2023/rapport2023_26.pdf, 2023.
- 818 Cannon, A.J., Sobie, S.R. and Murdock, T.Q.: Bias Correction of GCM Precipitation by Quantile Mapping: How Well Do
- Methods Preserve Changes in Quantiles and Extremes? Journal of Climate, 28, 6938-6959, https://doi.org/10.1175/JCLI-D-
- 820 <u>14-00754.1</u>, 2015.
- 821 CH2018: CH2018 Climate Scenarios for Switzerland, Technical Report. National Centre for Climate Services, Zürich, 271
- 822 pp, ISBN: 978-3-9525031-4-0, 2018.
- 823 Chinita, M. J., Richardson, M., Teixeira, J., and Miranda, P. M. A.: Global mean frequency increases of daily and sub-daily
- heavy precipitation in ERA5, Environ. Res. Lett., 16, 074035, https://doi.org/10.1088/1748-9326/ac0caa, 2021.
- Dalelane, C., Früh, B., Steger, C., and Walter, A.: A Pragmatic Approach to Build a Reduced Regional Climate Projection
- Ensemble for Germany Using the EURO-CORDEX 8.5 Ensemble, https://doi.org/10.1175/JAMC-D-17-0141.1, 2018.
- 827 DCCEEW: National Climate Risk Assessment: Methodology. Department of Climate Change, Energy, the Environment and
- Water, https://www.dcceew.gov.au/climate-change/publications/national-climate-risk-assessment, 2023.
- Dobler, A.: doblerone/3DBC: Version 2023 (Version v2023), Zenodo, https://doi.org/10.5281/zenodo.15260335, 2025.
- 830 Dobrowski, S. Z., Abatzoglou, J. T., Greenberg, J. A., and Schladow, S. G.: How much influence does landscape-scale
- physiography have on air temperature in a mountain environment?, Agricultural and Forest Meteorology, 149, 1751–1758,
- 832 <u>https://doi.org/10.1016/j.agrformet.2009.06.006</u>, 2009.
- Doherty, J. and Skahill, B. E.: An advanced regularization methodology for use in watershed model calibration, Journal of
- Hydrology, 327, 564–577, https://doi.org/10.1016/j.jhydrol.2005.11.058, 2006.
- Dunn, R. J. H., Alexander, L. V., Donat, M. G., Zhang, X., Bador, M., Herold, N., Lippmann, T., Allan, R., Aguilar, E., Barry,
- A. A., Brunet, M., Caesar, J., Chagnaud, G., Cheng, V., Cinco, T., Durre, I., de Guzman, R., Htay, T. M., Wan Ibadullah, W.
- M., Bin Ibrahim, M. K. I., Khoshkam, M., Kruger, A., Kubota, H., Leng, T. W., Lim, G., Li-Sha, L., Marengo, J., Mbatha, S.,
- McGree, S., Menne, M., de los Milagros Skansi, M., Ngwenya, S., Nkrumah, F., Oonariya, C., Pabon-Caicedo, J. D., Panthou,





- 639 G., Pham, C., Rahimzadeh, F., Ramos, A., Salgado, E., Salinger, J., Sané, Y., Sopaheluwakan, A., Srivastava, A., Sun, Y.,
- Timbal, B., Trachow, N., Trewin, B., van der Schrier, G., Vazquez-Aguirre, J., Vasquez, R., Villarroel, C., Vincent, L., Vischel,
- T., Vose, R., and Bin Hj Yussof, M. N.: Development of an Updated Global Land In Situ-Based Data Set of Temperature and
- 842 Precipitation Extremes: HadEX3, Journal of Geophysical Research: Atmospheres, 125, e2019JD032263,
- 843 https://doi.org/10.1029/2019JD032263, 2020.
- Dyrrdal, A.V., Bakke, S.J., Hanssen-Bauer, I., Mayer, S., Nilsen, I.B., Nilsen, J.E.Ø., Paasche, Ø., Saloranta, T., Årthun, M.
- 845 [editors]: Klima i Norge kunnskapsgrunnlag for klimatilpasning oppdatert i 2025 ("Climate in Norway knowledge base
- for climate adaptation updated in 2025"), NCCS Report 1/2025, Norwegian Centre for Climate Services, Oslo, Norway. (In
- 847 Norwegian.). https://doi.org/10.60839/4rgq-nn84, 2025.
- Eaton, B., Gregory, J., Drach, B., Taylor, K., Hankin, S., Caron, J., Signell, R., Bentley, P., Rappa, G., Höck, H., Pamment,
- A., Juckes, M., Raspaud, M., Blower, J., Horne, R., Whiteaker, T., Blodgett, D., Zender, C., Lee, D., Hassell, D., Snow, A. D.,
- Kölling, T., Allured, D., Jelenak, A. Soerensen, A. M., Gaultier, L., Herlédan, S.: NetCDF Climate and Forecast (CF) Metadata
- 851 Conventions (1.10). CF Community. https://doi.org/10.5281/zenodo.14275561, 2022.
- 852 EEA (European Environment Agency): Energy Performance of Buildings Directive.
- 853 https://energy.ec.europa.eu/topics/energy-efficiency/energy-performance-buildings/energy-performance-buildings-
- directive_en, last access: 19 August 2025.
- 855 Erlandsen, H. B., Tallaksen, L. M., and Kristiansen, J.: Merits of novel high-resolution estimates and existing long-term
- estimates of humidity and incident radiation in a complex domain, Earth System Science Data, 11, 797-821,
- 857 <u>https://doi.org/10.5194/essd-11-797-2019</u>, 2019.
- 858 Erlandsen, H. B., Parding, K. M., Benestad, R., Mezghani, A., and Pontoppidan, M.: A Hybrid Downscaling Approach for
- Future Temperature and Precipitation Change, https://doi.org/10.1175/JAMC-D-20-0013.1, 2020.
- 860 Erlandsen, H. B., Beldring, S., Eisner, S., Hisdal, H., Huang, S., and Tallaksen, L. M.: Constraining the HBV model for robust
- water balance assessments in a cold climate, Hydrology Research, 52, 356–372, https://doi.org/10.2166/nh.2021.132, 2021.
- 862 Eum, H.-I., Gupta, A., and Dibike, Y.: Effects of univariate and multivariate statistical downscaling methods on climatic and
- hydrologic indicators for Alberta, Canada, Journal of Hydrology, 588, 125065, https://doi.org/10.1016/j.jhydrol.2020.125065,
- 864 2020.





- Eyring, V., Bony, S., Meehl, G. A., Senior, C. A., Stevens, B., Stouffer, R. J., and Taylor, K. E.: Overview of the Coupled
- Model Intercomparison Project Phase 6 (CMIP6) experimental design and organization, Geoscientific Model Development,
- 9, 1937–1958, https://doi.org/10.5194/gmd-9-1937-2016, 2016.
- 868 Farahani, M. A., Wood, A. W., Tang, G., and Mizukami, N.: Calibrating a large-domain land/hydrology process model in the
- age of AI: the SUMMA CAMELS experiments, EGUsphere, 1–35, https://doi.org/10.5194/egusphere-2025-38, 2025.
- Fischer, A. M., Strassmann, K. M., Croci-Maspoli, M., Hama, A. M., Knutti, R., Kotlarski, S., Schär, C., Schnadt Poberaj, C.,
- Ban, N., Bavay, M., Beyerle, U., Bresch, D. N., Brönnimann, S., Burlando, P., Casanueva, A., Fatichi, S., Feigenwinter, I.,
- Fischer, E. M., Hirschi, M., Liniger, M. A., Marty, C., Medhaug, I., Peleg, N., Pickl, M., Raible, C. C., Rajczak, J., Rössler,
- O., Scherrer, S. C., Schwierz, C., Seneviratne, S. I., Skelton, M., Sørland, S. L., Spirig, C., Tschurr, F., Zeder, J., and Zubler,
- 874 E. M.: Climate Scenarios for Switzerland CH2018 Approach and Implications, Climate Services, 26, 100288,
- 875 https://doi.org/10.1016/j.cliser.2022.100288, 2022.
- François, B., Vrac, M., Cannon, A. J., Robin, Y., and Allard, D.: Multivariate bias corrections of climate simulations: which
- 877 benefits for which losses?, Earth System Dynamics, 11, 537–562, https://doi.org/10.5194/esd-11-537-2020, 2020.
- 878 Franke, J.: Rainfall complexity in mountains, Nat. Clim. Chang., 14, 1223–1223, https://doi.org/10.1038/s41558-024-02209-
- 879 <u>6, 2024.</u>
- Frei, C., Christensen, J. H., De'que', M., Jacob, D., Jones, R. G., and Vidale, P. L.: Daily precipitation statistics in regional
- 881 climate models: Evaluation and intercomparison for the European Alps. J. Geophys. Res., 108, 4124,
- 882 <u>https://doi.org/10.1029/2002JD002287</u>, 2003.
- 883 Gaarder, J.E., Tajet, H.T.T., Dobler, A., Hygen, H.O. and Kvande, T.: Future Climate Projections and Uncertainty Evaluations
- for Frost Decay Exposure Index in Norway. Buildings, 14(9), p.2873, https://doi.org/10.3390/buildings14092873, 2024
- 685 Golding, N., Lambkin, K., Wilson, L., Troch, R. D., Fischer, A. M., Hygen, H. O., Hama, A. M., Dyrrdal, A. V., Jamsin, E.,
- 886 Termonia, P., and Hewitt, C.: Developing national frameworks for climate services: Experiences, challenges and learnings
- from across Europe, Climate Services, 37, 100530, https://doi.org/10.1016/j.cliser.2024.100530, 2025.
- 888 Gjertsen, A.K. and Nilsen, J.E.: SAT-SKOG: Et skogkart basert på tolking av satellittbilder. Skog og landskap, rapport nr.
- 889 23/2012, 54 pp, http://hdl.handle.net/11250/2453917 2012.
- 890 Gu, G. and Adler, R. F.: Spatial Patterns of Global Precipitation Change and Variability during 1901-2010,
- 891 <u>https://doi.org/10.1175/JCLI-D-14-00201.1, 2015.</u>





- 892 Gudmundsson, L.: qmap: Statistical Transformations for Post-Processing Climate Model Output, version 1.0-6,
- https://doi.org/10.32614/CRAN.package.qmap, 2025.
- 694 Gudmundsson, L., Bremnes, J. B., Haugen, J. E., and Engen-Skaugen, T.: Technical Note: Downscaling RCM precipitation to
- the station scale using statistical transformations a comparison of methods, Hydrology and Earth System Sciences,
- 896 16, 3383–3390, https://doi.org/10.5194/hess-16-3383-2012, 2012.
- 697 Gudmundsson, L., Boulange, J., Do, H. X., Gosling, S. N., Grillakis, M. G., Koutroulis, A. G., Leonard, M., Liu, J., Müller
- 898 Schmied, H., Papadimitriou, L., Pokhrel, Y., Seneviratne, S. I., Satoh, Y., Thiery, W., Westra, S., Zhang, X., and Zhao, F.:
- 899 Globally observed trends in mean and extreme river flow attributed to climate change, Science, 371, 1159-1162,
- 900 <u>https://doi.org/10.1126/science.aba3996</u>, 2021.
- 901 Gutiérrez, J. M., Maraun, D., Widmann, M., Huth, R., Hertig, E., Benestad, R., Roessler, O., Wibig, J., Wilcke, R., Kotlarski,
- 902 S., San Martín, D., Herrera, S., Bedia, J., Casanueva, A., Manzanas, R., Iturbide, M., Vrac, M., Dubrovsky, M., Ribalaygua,
- J., Pórtoles, J., Räty, O., Räisänen, J., Hingray, B., Raynaud, D., Casado, M. J., Ramos, P., Zerenner, T., Turco, M., Bosshard,
- T., Štěpánek, P., Bartholy, J., Pongracz, R., Keller, D. E., Fischer, A. M., Cardoso, R. M., Soares, P. M. M., Czernecki, B.,
- 905 and Pagé, C.: An intercomparison of a large ensemble of statistical downscaling methods over Europe: Results from the
- 906 VALUE perfect predictor cross-validation experiment, International Journal of Climatology, 39, 3750–3785,
- 907 https://doi.org/10.1002/joc.5462, 2019.
- 908 Hanssen-Bauer, I., Benestad, R.E., Lutz, J., Vikhamar-Schuler, D., Svyashchennikov, P. and Førland, E.J: Comparative
- Analyses of Local Historical and Future Climate Conditions Important for Reindeer Herding in Finnmark, Norway and the
- Yamal Nenets Autonomous Okrug, Russia. In: Mathiesen, S.D., Eira, I.M.G., Turi, E.I., Oskal, A., Pogodaev, M., Tonkopeeva,
- 911 M. (eds) Reindeer Husbandry. Springer Polar Sciences. Springer, Cham. https://doi.org/10.1007/978-3-031-17625-8 8, 2022
- 912 Hanssen-Bauer, I., E.J. Førland, I. Haddeland, H. Hisdal, S. Mayer, A. Nesje, J. E. Ø. Nilsen, S. Sandven, A. B. Sandø, A. Sorteberg
- 913 og B.Ådlandsvik, Klima i Norge 2100 Kunnskapsgrunnlag for klimatilpasning oppdatert i 2015. Norsk Klimaservicesenter,
- 914 NCCS Report 2/2015 203pp. ISSN: 2387-3027, 2015.
- Hawkins, E. and Sutton, R.: The potential to narrow uncertainty in projections of regional precipitation change, Clim Dyn, 37,
- 916 407–418, https://doi.org/10.1007/s00382-010-0810-6, 2011.
- 917 Hisdal, H., Vikhamar-Schuler, D., Førland, E., and Nilsen, I. (2021). Klimaprofiler for fylker. ("Climate factsheets for
- 918 counties"). NCCS Report 2/2021, Norwegian Centre for Climate Services, Oslo, Norway. (In Norwegian.).
- 919 https://klimaservicesenter.no/kss/rapporter/rapporter-og-publikasjoner-2





- Huang, S., Eisner, S., Magnusson, J. O., Lussana, C., Yang, X., and Beldring, S.: Improvements of the spatially distributed
- 921 hydrological modelling using the HBV model at 1 km resolution for Norway, Journal of Hydrology, 577, 123585,
- 922 https://doi.org/10.1016/j.jhydrol.2019.03.051, 2019.
- Huang, S., Eisner, S., Haddeland, I., and Tadege Mengistu, Z.: Evaluation of two new-generation global soil databases for
- 924 macro-scale hydrological modelling in Norway, Journal of Hydrology, 610, 127895,
- 925 https://doi.org/10.1016/j.jhydrol.2022.127895, 2022.
- 926 Huang, S., Haddeland, I., Lussana, C., Dobler, A., and Tveito, O.E.: Daily climate and hydrological reference data for Norway
- 927 [Data set]. Dataset published 2025 via Norwegian Meteorological Institute, https://doi.org/10.21343/gbq0-4t97, 2025
- Hundecha, Y., Sunyer, M. A., Lawrence, D., Madsen, H., Willems, P., Bürger, G., Kriaučiūnienė, J., Loukas, A., Martinkova,
- 929 M., Osuch, M., Vasiliades, L., von Christierson, B., Vormoor, K., and Yücel, I.: Inter-comparison of statistical downscaling
- 930 methods for projection of extreme flow indices across Europe, Journal of Hydrology, 541, 1273-1286,
- 931 https://doi.org/10.1016/j.jhydrol.2016.08.033, 2016.
- Huss, M., Jouvet, G., Farinotti, D., and Bauder, A.: Future high-mountain hydrology: a new parameterization of glacier retreat,
- 933 Hydrology and Earth System Sciences, 14, 815–829, https://doi.org/10.5194/hess-14-815-2010, 2010.
- 934 IPCC: Climate Change 2021: The Physical Science Basis. Contribution of Working Group I to the Sixth Assessment Report
- 935 of the Intergovernmental Panel on Climate Change Masson-Delmotte, V., P. Zhai, A. Pirani, S.L. Connors, C. Péan, S. Berger,
- 936 N. Caud, Y. Chen, L. Goldfarb, M.I. Gomis, M. Huang, K. Leitzell, E. Lonnoy, J.B.R. Matthews, T.K. Maycock, T. Waterfield,
- O. Yelekçi, R. Yu, and B. Zhou (eds.)]. Cambridge University Press, Cambridge, United Kingdom and New York, NY, USA,
- 938 In press, doi:10.1017/9781009157896, 2021.
- Jacob, D., Petersen, J., Eggert, B., Alias, A., Christensen, O. B., Bouwer, L. M., Braun, A., Colette, A., Déqué, M., Georgievski,
- 940 G., Georgopoulou, E., Gobiet, A., Menut, L., Nikulin, G., Haensler, A., Hempelmann, N., Jones, C., Keuler, K., Kovats, S.,
- 941 Kröner, N., Kotlarski, S., Kriegsmann, A., Martin, E., van Meijgaard, E., Moseley, C., Pfeifer, S., Preuschmann, S.,
- Radermacher, C., Radtke, K., Rechid, D., Rounsevell, M., Samuelsson, P., Somot, S., Soussana, J.-F., Teichmann, C.,
- 943 Valentini, R., Vautard, R., Weber, B., and Yiou, P.: EURO-CORDEX: new high-resolution climate change projections for
- 944 European impact research, Reg Environ Change, 14, 563–578, https://doi.org/10.1007/s10113-013-0499-2, 2014.
- Jacob, D., Teichmann, C., Sobolowski, S., Katragkou, E., Anders, I., Belda, M., Benestad, R., Boberg, F., Buonomo, E.,
- Cardoso, R. M., Casanueva, A., Christensen, O. B., Christensen, J. H., Coppola, E., De Cruz, L., Davin, E. L., Dobler, A.,
- 947 Domínguez, M., Fealy, R., Fernandez, J., Gaertner, M. A., García-Díez, M., Giorgi, F., Gobiet, A., Goergen, K., Gómez-
- 948 Navarro, J. J., Alemán, J. J. G., Gutiérrez, C., Gutiérrez, J. M., Güttler, I., Haensler, A., Halenka, T., Jerez, S., Jiménez-





- Guerrero, P., Jones, R. G., Keuler, K., Kjellström, E., Knist, S., Kotlarski, S., Maraun, D., van Meijgaard, E., Mercogliano, P.,
- 950 Montávez, J. P., Navarra, A., Nikulin, G., de Noblet-Ducoudré, N., Panitz, H.-J., Pfeifer, S., Piazza, M., Pichelli, E.,
- 951 Pietikäinen, J.-P., Prein, A. F., Preuschmann, S., Rechid, D., Rockel, B., Romera, R., Sánchez, E., Sieck, K., Soares, P. M. M.,
- Somot, S., Srnec, L., Sørland, S. L., Termonia, P., Truhetz, H., Vautard, R., Warrach-Sagi, K., and Wulfmeyer, V.: Regional
- 953 climate downscaling over Europe: perspectives from the EURO-CORDEX community, Reg Environ Change, 20, 51,
- 954 https://doi.org/10.1007/s10113-020-01606-9, 2020.
- 955 Katragkou, E., Sobolowski, S.P., Teichmann, C., Solmon, F., Pavlidis, V., Rechid, D., Hoffmann, P., Fernández, J., Nikulin,
- 956 G. and Jacob, D.: Delivering an improved framework for the new generation of CMIP6-driven EURO-CORDEX regional
- climate simulations. Bulletin of the American Meteorological Society, 105(6), pp.E962-E974, https://doi.org/10.1175/BAMS-
- 958 <u>D-23-0131.1</u>, 2024.
- 959 Kundzewicz, Z. W., Krysanova, V., Dankers, R., Hirabayashi, Y., Kanae, S., Hattermann, F. F., Huang, S., Milly, P. C. D.,
- 960 Stoffel, M., Driessen, P. P. J., Matczak, P., Quevauviller, P., and Schellnhuber, H.-J.: Differences in flood hazard projections
- 961 in Europe their causes and consequences for decision making, Hydrological Sciences Journal, 62, 1–14,
- 962 https://doi.org/10.1080/02626667.2016.1241398, 2017.
- 963 Kuya, E. K., Hanssen-Bauer, I., Mayer, S., and Heiberg, H.: Projected changes of rain, sleet, and snowfall in Norway, Norsk
- 964 Geografisk Tidsskrift Norwegian Journal of Geography, 78, 73–87, https://doi.org/10.1080/00291951.2024.2360409, 2024.
- 965 Lafferty, D. C. and Sriver, R. L.: Downscaling and bias-correction contribute considerable uncertainty to local climate
- projections in CMIP6, npj Clim Atmos Sci, 6, 158, https://doi.org/10.1038/s41612-023-00486-0, 2023.
- 967 Lawrence, D.: Uncertainty introduced by flood frequency analysis in projections for changes in flood magnitudes under a
- 968 future climate in Norway. Journal of Hydrology: Regional Studies 28:100675, https://doi.org/10.1016/j.ejrh.2020.100675,
- 969 2020.
- 970 Li, H., Beldring, S., Xu, C.-Y., Huss, M., Melvold, K., and Jain, S. K.: Integrating a glacier retreat model into a hydrological
- 971 model Case studies of three glacierised catchments in Norway and Himalayan region, Journal of Hydrology, 527, 656–667,
- 972 https://doi.org/10.1016/j.jhydrol.2015.05.017, 2015.
- Li, L., Wang, B., Feng, P., Jägermeyr, J., Asseng, S., Müller, C., Macadam, I., Liu, D. L., Waters, C., Zhang, Y., He, Q., Shi,
- 974 Y., Chen, S., Guo, X., Li, Y., He, J., Feng, H., Yang, G., Tian, H., and Yu, Q.: The optimization of model ensemble composition
- and size can enhance the robustness of crop yield projections, Commun Earth Environ, 4, 362, https://doi.org/10.1038/s43247-
- 976 023-01016-9, 2023.





- 977 Lussana, C: seNorge observational gridded datasets, MET report 7-2020, https://www.met.no/publikasjoner/met-report/met-
- 978 report-2020/ /attachment/download/9f79d391-62d8-4fc1-a61a-
- 979 9f0e7f1de389:8c74ebf2118593aa75272e6aff416ce66f86e73f/MET-report-07-2020.pdf, 2020.
- 980 Lussana, C., Tveito, O. E., Dobler, A., and Tunheim, K.: seNorge 2018, daily precipitation, and temperature datasets over
- Norway, Earth System Science Data, 11, 1531–1551, https://doi.org/10.5194/essd-11-1531-2019, 2019.
- 982 Lutz, J., Hanssen-Bauer, I., Tveito, O. E. and Dobler, A.: Precipitation variability in Norway 1961–2020. MET-report 01-
- 983 2024, https://www.met.no/publikasjoner/met-report/ /attachment/download/f5ba4d69-dba2-4eb6-bed9-
- 984 0189178b5e7a:ba4f4974e503f9509d33f101efc40145b47a59e6/MET%20report%201%202024.pdf, 2024.
- 985 Majasalmi, T., Eisner, S., Astrup, R., Fridman, J., and Bright, R. M.: An enhanced forest classification scheme for modeling
- vegetation-climate interactions based on national forest inventory data, Biogeosciences, 15, 399–412,
- 987 <u>https://doi.org/10.5194/bg-15-399-2018</u>, 2018.
- Martinich, J. and Crimmins, A.: Climate damages and adaptation potential across diverse sectors of the United States, Nature
- 989 Climate Change, 9, 397-404, 2019.
- Mayer, S., Khasandi Kuya, E., Antonsen, K., Abegg, B., and Hanssen-Bauer, I.: Warmer and wetter: Outlining climate services
- 991 for snow-dependent tourism in Norway The case of Lofoten, Climate Services, 32, 100405,
- 992 https://doi.org/10.1016/j.cliser.2023.100405, 2023.
- 993 McAfee, S. A.: Methodological differences in projected potential evapotranspiration, Climatic Change, 120, 915–930,
- 994 https://doi.org/10.1007/s10584-013-0864-7, 2013.
- 995 Maraun, D. and Widmann, M.: Statistical Downscaling and Bias Correction for Climate Research. Cambridge University
- 996 Press, 347 pp, 2018.
- 997 McSweeney, C. F., Jones, R. G., Lee, R. W., and Rowell, D. P.: Selecting CMIP5 GCMs for downscaling over multiple
- 998 regions, Clim Dyn, 44, 3237–3260, https://doi.org/10.1007/s00382-014-2418-8, 2015.
- 999 Mehrotra, R. and Sharma, A.: A Resampling Approach for Correcting Systematic Spatiotemporal Biases for Multiple Variables
- in a Changing Climate, Water Resources Research, 55, 754–770, https://doi.org/10.1029/2018WR023270, 2019.
- 1001 Meyer, J., Kohn, I., Stahl, K., Hakala, K., Seibert, J., and Cannon, A. J.: Effects of univariate and multivariate bias correction
- on hydrological impact projections in alpine catchments, Hydrol. Earth Syst. Sci., 23, 1339–1354, https://doi.org/10.5194/hess-
- 1003 23-1339-2019, 2019.





- Moriasi, D. N., Arnold, J. G., Liew, M. W. V., Bingner, R. L., Harmel, R. D., and Veith, T. L.: Model Evaluation Guidelines
- 1005 for Systematic Quantification of Accuracy in Watershed Simulations, Transactions of the ASABE, 50, 885-900,
- 1006 https://doi.org/10.13031/2013.23153, 2007.
- 1007 Müller, M., Homleid, M., Ivarsson, K.-I., Køltzow, M. A. Ø., Lindskog, M., Midtbø, K. H., Andrae, U., Aspelien, T., Berggren,
- 1008 L., Bjørge, D., Dahlgren, P., Kristiansen, J., Randriamampianina, R., Ridal, M., and Vignes, O.: AROME-MetCoOp: A Nordic
- 1009 Convective-Scale Operational Weather Prediction Model, https://doi.org/10.1175/WAF-D-16-0099.1, 2017.
- 1010 Nash, J.E. and Sutcliffe, J.V.: River flow forecasting through conceptual models part I -A discussion of principles, J Hydrol,
- 1011 10, 282–290, 1970.
- Nilsen, I. B., Hanssen-Bauer, I., Tveito, O. E., and Wong, W. K.: Projected changes in days with zero-crossings for Norway,
- 1013 International Journal of Climatology, 41, 2173–2188, https://doi.org/10.1002/joc.6913, 2021.
- Nilsen, I. B., Hanssen-Bauer, I., Dyrrdal, A. V., Hisdal, H., Lawrence, D., Haddeland, I., and Wong, W. K.: From Climate
- 1015 Model Output to Actionable Climate Information in Norway, Front. Clim., 4, https://doi.org/10.3389/fclim.2022.866563,
- 1016 2022.
- 1017 Norwegian Government (2024). Statlige Planretningslinjer for klima- og energi. ("government guidelines on climate and
- 1018 renergy"). Available online at: https://lovdata.no/dokument/SF/forskrift/2024-12-20-3359 (accessed December 06. October
- 1019 2025).
- Padrón, R. S., Gudmundsson, L., Decharme, B., Ducharne, A., Lawrence, D. M., Mao, J., Peano, D., Krinner, G., Kim, H.,
- and Seneviratne, S. I.: Observed changes in dry-season water availability attributed to human-induced climate change, Nat.
- 1022 Geosci., 13, 477–481, https://doi.org/10.1038/s41561-020-0594-1, 2020.
- 1023 Peter, J., Vogel, E., Sharples, W., Bende-Michl, U., Wilson, L., Hope, P., Dowdy, A., Kociuba, G., Srikanthan, S., Duong, V.
- 1024 C., Roussis, J., Matic, V., Khan, Z., Oke, A., Turner, M., Baron-Hay, S., Johnson, F., Mehrotra, R., Sharma, A., Thatcher, M.,
- 1025 Azarvinand, A., Thomas, S., Boschat, G., Donnelly, C., and Argent, R.: Continental-scale bias-corrected climate and
- hydrological projections for Australia, Geoscientific Model Development, 17, 2755–2781, https://doi.org/10.5194/gmd-17-
- 1027 2755-2024, 2024.
- 1028 Pirk, N., Aalstad, K., Yilmaz, Y. A., Vatne, A., Popp, A. L., Horvath, P., Bryn, A., Vollsnes, A. V., Westermann, S., Berntsen,
- 1029 T. K., Stordal, F., and Tallaksen, L. M.: Snow-vegetation-atmosphere interactions in alpine tundra, Biogeosciences, 20, 2031-
- 1030 2047, https://doi.org/10.5194/bg-20-2031-2023, 2023.





- 1031 Pourmokhtarian, A., Driscoll, C. T., Campbell, J. L., Hayhoe, K., and Stoner, A. M. K.: The effects of climate downscaling
- technique and observational data set on modeled ecological responses, Ecological Applications, 26, 1321-1337,
- 1033 https://doi.org/10.1890/15-0745, 2016.
- Reistad, M., Øyvind Breivik, Haakenstad, H., Aarnes, O. J., Furevik, B. R., and Bidlot, J.-R.: A high-resolution hindcast of
- 1035 wind and waves for the North Sea, the Norwegian Sea, and the Barents Sea, J. Geophys. Res., 116,
- 1036 https://doi.org/10.1029/2010JC006402, 2011.
- 1037 Reyniers, N., Zha, Q., Addor, N., Osborn, T. J., Forstenhäusler, N., and He, Y.: Two sets of bias-corrected regional UK Climate
- 1038 Projections 2018 (UKCP18) of temperature, precipitation and potential evapotranspiration for Great Britain, Earth System
- 1039 Science Data, 17, 2113–2133, https://doi.org/10.5194/essd-17-2113-2025, 2025.
- 1040 Rössler, O., Fischer, A. M., Huebener, H., Maraun, D., Benestad, R. E., Christodoulides, P., Soares, P. M. M., Cardoso, R. M.,
- 1041 Pagé, C., Kanamaru, H., Kreienkamp, F., and Vlachogiannis, D.: Challenges to link climate change data provision and user
- 1042 needs: Perspective from the COST-action VALUE, International Journal of Climatology, 39, 3704–3716,
- 1043 https://doi.org/10.1002/joc.5060, 2019.
- 1044 Statistics Norway: Land use and land cover SSB, last accessed on 27.03.2025.
- 1045 Schumacher, D.L., Singh, J., Hauser, M., Fischer, E.M., Wild, M. and Seneviratne, S.I.:. Exacerbated summer European
- 1046 warming not captured by climate models neglecting long-term aerosol changes. Communications Earth & Environment, 5(1),
- 1047 p.182, https://doi.org/10.1038/s43247-024-01332-8, 2024.
- 1048 Tam, B., Bonsal, B., Zhang, X., Zhang, Q., and Rong, R.: Assessing Potential Evapotranspiration Methods in Future Drought
- 1049 Projections across Canada, Atmosphere-Ocean, 62, 193–205, https://doi.org/10.1080/07055900.2023.2288632, 2024.
- Tang, J., Niu, X., Wang, S., Gao, H., Wang, X., and Wu, J.: Statistical downscaling and dynamical downscaling of regional
- 1051 climate in China: Present climate evaluations and future climate projections, Journal of Geophysical Research: Atmospheres,
- 1052 121, 2110–2129, https://doi.org/10.1002/2015JD023977, 2016.
- 1053 Taylor, K. E., Stouffer, R. J., and Meehl, G. A.: An overview of CMIP5 and the experiment design, B. Am. Meteorol. Soc.,
- 1054 93, 485–498, https://doi.org/10.1175/BAMS-D-11-00094.1, 2012.
- 1055 Taylor, K. E., Stouffer, R. J., and Meehl, G. A.: An Overview of CMIP5 and the Experiment Design,
- 1056 https://doi.org/10.1175/BAMS-D-11-00094.1, 2012.





- 1057 Thorarinsdottir, T. L., Gneiting, T., and Gissibl, N.: Using proper divergence functions to evaluate climate models. SIAM-
- 1058 ASA J. Uncertainty Quantif., 1, 522–534, https://doi.org/10.1137/130907550, 2013.
- 1059 Tveito, O. E.: Norwegian standard climate normals 1991-2020 the methodological approach, MET report 5 2021,
- https://www.met.no/publikasjoner/met-report/met-report-2021/ /attachment/download/31bb0160-d8cf-4a2b-9646-
- 4df6f5904059:3ac4fec6cf3fb7919aefe42db2b63ad8e8b9e6a6/METreport%2005_2021_New_Norwegian_standard_climate_
- normals_1991_2020-signert.pdf, 2021.
- Vautard, R., Kadygrov, N., Iles, C., Boberg, F., Buonomo, E., Bülow, K., Coppola, E., Corre, L., van Meijgaard, E.,
- Nogherotto, R., Sandstad, M., Schwingshackl, C., Somot, S., Aalbers, E., Christensen, O. B., Ciarlo, J. M., Demory, M.-E.,
- 1065 Giorgi, F., Jacob, D., Jones, R. G., Keuler, K., Kjellström, E., Lenderink, G., Levavasseur, G., Nikulin, G., Sillmann, J.,
- 1066 Solidoro, C., Sørland, S. L., Steger, C., Teichmann, C., Warrach-Sagi, K., and Wulfmeyer, V.: Evaluation of the Large EURO-
- 1067 CORDEX Regional Climate Model Ensemble, Journal of Geophysical Research: Atmospheres, 126, e2019JD032344,
- 1068 https://doi.org/10.1029/2019JD032344, 2021.
- Wang, X. and Liu, L.: The Impacts of Climate Change on the Hydrological Cycle and Water Resource Management, Water,
- 1070 15, 2342, https://doi.org/10.3390/w15132342, 2023.
- Wolff, M. A., Isaksen, K., Petersen-Øverleir, A., Ødemark, K., Reitan, T., and Brækkan, R.: Derivation of a new continuous
- adjustment function for correcting wind-induced loss of solid precipitation: results of a Norwegian field study, Hydrology and
- 1073 Earth System Sciences, 19, 951–967, https://doi.org/10.5194/hess-19-951-2015, 2015.
- 1074 Wong, W.K., Dobler, A., Huang, S., Beldring, S., Melvold, K., Ruan, G.: Daily bias-adjusted climate (COR-BA-2025) and
- 1075 hydrological (distHBV-COR-BA-2025) projections for Norway [Data set]. Dataset published 2025 via Norwegian
- 1076 Meteorological Institute https://doi.org/10.21343/0k90-6w67, 2025
- 1077 Wong, W.K., Haddeland, I., Lawrence, D., and Beldring, S.: Gridded 1x1 km climate and hydrological projections for Norway.
- 1078 NVE Report No. 59, Norwegian Water Resources and Energy Directorate, Oslo, Norway, 2016.
- 1079 Yilmaz, K. K., Gupta, H. V., and Wagener, T.: A process-based diagnostic approach to model evaluation: Application to the
- NWS distributed hydrologic model, Water Resources Research, 44, https://doi.org/10.1029/2007WR006716, 2008.
- 1081 Yuan, Q., Thorarinsdottir, T. L., Beldring, S., Wong, W. K., Huang, S., and Xu, C.-Y.: New Approach for Bias Correction and
- 1082 Stochastic Downscaling of Future Projections for Daily Mean Temperatures to a High-Resolution Grid, J. Appl. Meteorol.
- 1083 Clim., 58, 2617–2632, https://doi.org/10.1175/JAMC-D-19-0086.1, 2019.



1084

1090



stochastic simulations of gridded daily precipitation in a future climate, Hydrol. Earth Syst. Sci., 25 (9), pp. 5259-5275, https://doi.org/10.5194/hess-25-5259-2021, 2021.

Zhang, L., Xu, Y., Meng, C., Li, X., Liu, H., and Wang, C.: Comparison of Statistical and Dynamic Downscaling Techniques in Generating High-Resolution Temperatures in China from CMIP5 GCMs, https://doi.org/10.1175/JAMC-D-19-0048.1, 2020.

Yuan Q., Thorarinsdottir T.L., Beldring S., Wong W.K., and Xu C.-Y.: Bridging the scale gap: obtaining high-resolution

51